Physics and Chemistry of the Earth 123 (2021) 103029

Contents lists available at ScienceDirect

Physics and Chemistry of the Earth

journal homepage: www.elsevier.com/locate/pce

A hybrid probabilistic seismic hazard model for Northeast India and Bhutan combining distributed seismicity and finite faults

Federica Ghione [a,d,*], Valerio Poggi [b], Conrad Lindholm [c]

[a] NORSAR, Gunnar Randers Vei 15, 2007, Kjeller, Norway
[b] Seismological Research Center, National Institute of Oceanography and Applied Geophysics (OGS), Via Treviso, 55, 33100, Udine, Italy
[c] SeismoConsult, Fjellhamar, Norway
[d] Department of Geosciences, University of Oslo, Norway

ARTICLE INFO

Keywords:
Northeast India
Bhutan
Probabilistic seismic hazard analysis
Distributed seismicity
Finite faults

ABSTRACT

In Probabilistic Seismic Hazard Analysis (PSHA), a widely used approach to model earthquake sources consists of using homogenous source zones. This approach suffers the limitation of assuming that the observed seismicity can occur anywhere with same probability over a specific area, which might lead to the potential undervaluation of the predicted ground motion level due to an effect of smearing of seismic potential. To compensate that, a hybrid model is used, accounting both for distributed seismicity and localized seismogenic structures.

In this study, we perform PSHA for Northeast India and Bhutan, that are the most seismically hazardous regions on the planet. The region was partitioned into seismogenic source zones of supposedly homogeneous seismic potential and seismotectonic characteristics. Earthquake recurrence parameters for each zone were obtained from direct magnitude-frequency analysis on a precompiled global catalogue. Seismogenic faults are added to the model by converting slip rates from GPS velocity data to seismic activity. Complementary information was derived from the analysis of moment tensor solutions of large events and from a detailed literature review.

Using this hybrid model, seismic hazard was calculated for a region bounded by lat/long 24.0°-28.8°N/88.0°-94.5°E. Calculations were performed for Peak Ground Acceleration (PGA) and several Spectral Acceleration (SA) periods for a Probability of Exceedance (POE) of 10% in 50 years, corresponding to 475 years return period, and for a reference rock condition with Vs = 800 m/s. The results highlight significant acceleration levels (about 0.77g at PGA) in the Arunachal Pradesh region (Northeast India), due to the presence of the Himalayan Frontal Thrust (HFT).

1. Introduction

Northeast India and Bhutan are one of the most active seismotectonic regions of the world (Baro and Kumar, 2017; Baruah et al., 2016) and over the last decades, different kinematic models have been proposed to explain the seismotectonics of the area. The area considered for the analysis lies between latitude 23°N to 30°N and longitude 85°E to 98°E (Fig. 1). From the geographical point of view, the study area is bounded by the Himalayas to the north, the Indo-Burma ranges/Myanmar to the east, Bangladesh to the southwest and the Andaman Sumatra region to the southeast. The geology of this region is complex with the interaction between the active north-south convergence along the Himalaya and the east-west convergence and subduction within the Indo-Burma ranges.

Historically, the study region is strongly affected by earthquakes with large magnitudes: during the past 120 years, thirteen events with magnitude above 7.0 have occurred in the study area (Baro and Kumar, 2017; Kayal, 2008; see Fig. 1). The main purpose of this work is to evaluate probabilistically the level of ground motion induced by large and potentially damaging future earthquakes in the densely populated region of Northeast India and Bhutan, which is fundamental to mitigate the impact of future events on the population and therefore to reduce the seismic risk. We use a Probabilistic Seismic Hazard Analysis (PSHA) approach (Cornell, 1968; Esteva, 1967, 1968), which allows to define the probability of a specified ground motion level being exceeded at a site or area of interest, as generated by any earthquake source potentially expected for the region. The way the earthquake source is

* Corresponding author. NORSAR, Gunnar Randers Vei 15, 2007, Kjeller, Norway.
E-mail addresses: federica.ghione@norsar.no (F. Ghione), vpoggi@inogs.it (V. Poggi), conrad.lindholm@outlook.com (C. Lindholm).

https://doi.org/10.1016/j.pce.2021.103029
Received 2 November 2020; Received in revised form 12 March 2021; Accepted 10 May 2021
Available online 17 May 2021

modelled, therefore, plays a major role in the analysis and has a significant impact on the final results.

The most common approach to model the earthquake source is using a distributed seismicity approach, where the study area is subdivided in a number of homogeneous zones (from the seismotectonics point of view), where each point is assumed to have the same probability of generating an earthquake. The seismic productivity (activity rates) is calibrated from the analysis of all the available observed events (e.g. from an earthquake catalogue) on the area, assuming a given magnitude-recurrence relation. This approach is convenient when little knowledge about the seismic sources is available for the region, but might be limiting in case of known active lineaments with large seismogenic potential. A more recent and sophisticated approach consists then in the direct modelling of the main active faults of the region (Akinci et al., 2009; Carlton et al., 2018; Poggi et al., 2020; Rivas-Medina et al., 2018; Valentini et al., 2017; Woessner et al., 2015; Yaghmaei-Sabegh et al., 2018). As for the case of source zones, occurrence on a fault can be calibrated by analysing the associated historical earthquake record that, however, might be rather limited in time for the specific lineament. To compensate for this, slip rates from geological or geodetical analysis (e.g. from strain rates) can also be used to model earthquake occurrences. Nonetheless, also this approach is affected by several limitations. Slip rates, for example, might be affected by large uncertainty and the assumption of stationarity of the deformation rate over long time periods might not be necessarily fulfilled.

Previous studies on the same area have used the classic area source model to compute the PSHA (Baro et al., 2020; 2018; Bhatia et al., 1999; Das et al., 2016; Giardini et al., 1999; Khattri et al., 1984; Nath and Thingbaijam, 2012; NDMA, 2011; Sharma and Malik, 2006; Shivamanth et al., 2016; Walling and Mohanty, 2009; Yadav et al., 2010); a recent study from Stevens et al. (2020) has performed a PSHA based on faults locations, slip-rates and paleoseismic earthquake data for Bhutan.

The purpose of the present investigation is therefore to create a hybrid model for Northeast India and Bhutan, which comprises classical area source zones and faults sources, in order to compensate the relative limitations of the two approaches and thereby to obtain a more comprehensive representation of the seismic hazard of the area. For that, we make extensive use of the slip rate information available in literature for local studies (Barman et al., 2017; Bilham and England, 2001; De and Kayal, 2003; Diehl et al., 2017; England and Bilham, 2015; Goswami, 2005; Hauck et al., 1998; Hetényi et al., 2016; Kayal et al., 2006; Le Roux-Mallouf et al., 2015; Marechal et al., 2016; Nandy, 2001; Stevens et al., 2020; Stevens and Avouac, 2015; Velasco et al., 2007; Vernant et al., 2014; Yin, 2006).

As a final result, we compute ground motion for 10% Probability of Exceedance (POE) in 50 years (corresponding to 475 years return period) for three target sites of particular significance for the area: Thimphu, Guwahati and Shillong. The obtained results can be used in the future to design earthquake resistant civil structures and define the earthquakes scenario for deterministic risk assessment.

2. Geology and Seismotectonics

Northeast India and Bhutan are among the seismically most active regions on earth. The high seismicity is due to the north-south collision between the Indian and the Eurasian plate along the Himalaya front, and the east-west subduction along the Indo-Burmese Ranges (IBR) in the east. The convergence of the Indian and Eurasian plates at 40–50 mm/yr since their initial collision between 70 and 34 million years ago resulted in the accumulation of widespread strain in the region. About 15–20 mm/yr of the convergence is accommodated in the Himalayan frontal arc (Vorobieva et al., 2017). The convergence along the entire Himalayan arc is directed perpendicular to the arc and increases eastwards from 13.3 ± 1.7 mm/yr in the west to 21.2 ± 2.0 mm/yr in the east (Stevens and Avouac, 2015).

Scientific debate is still ongoing about the identity and correlation of stratigraphic units, location and origin of the major contacts between the different units, and the timing of the orogenic processes in the region (Greenwood et al., 2016). There are also substantial differences in the geology between the western, eastern and central part of the Himalayas (Kayal, 2008). Based on the geology and the seismotectonics, we have divided the area into seven main provinces, which are discussed below.

2.1. Bhutan

The Bhutan region is characterized by the high topographic relief of the Himalaya, that is 2500 km-long along Himalayan belt and it is associated to several thrust and faults. Along the Main Himalayan Thrust

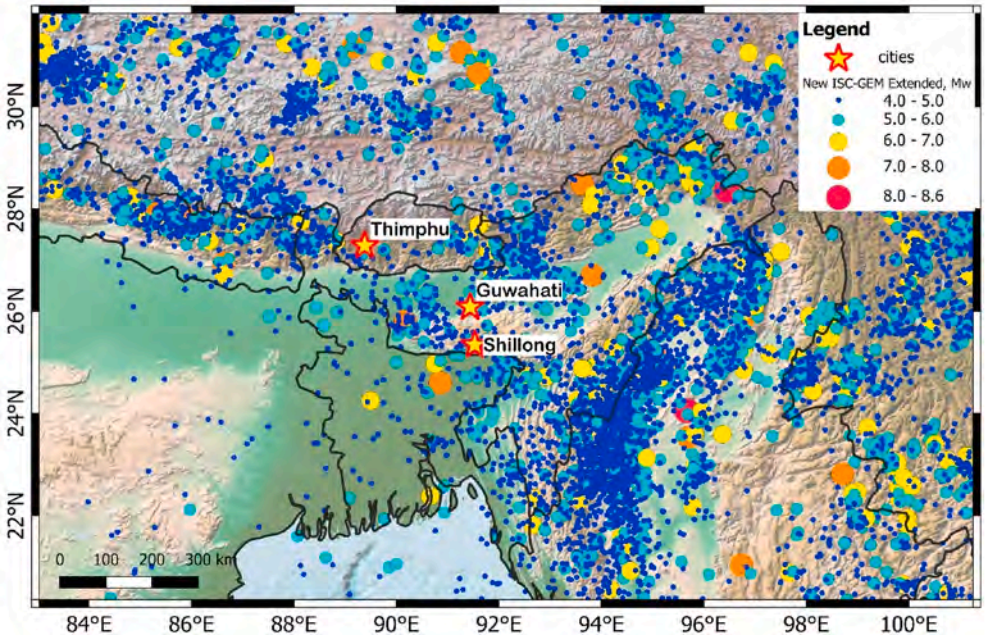

Fig. 1. The Mw homogenized earthquake catalogue (New ISC-GEM Extended) for the study region. The stars show the cities (Thimphu, Guwahati and Shillong) where the ground motion exceedance values are computed.

(MHT), which is a mid-crustal décollement (basal detachment fault), the Indian plate underthrusts the Eurasian plate, causing the Himalaya mountain growth and associated deformation and high seismicity. From north to south, the Main Central Thrust (MCT), the Main Boundary Thrust (MBT) and the Main Frontal Thrust (MFT) are the prominent north dipping thrusts with a geometry that is listric to the MHT (see Fig. 2). The MFT, also known as Himalayan Frontal Thrust (HFT), is considered as the surface expression of the MHT, the outermost front toward south and it runs along the Bhutan/India border (Barman et al., 2017). While the MFT is well defined in Nepal, in Bhutan it does not have a continuous and clear morphological expression because it is buried under young alluvial sediments.

Along the Himalayan arc, the seismic behaviour of the Bhutan region is uncertain, because the number of significant earthquakes in Bhutan is much lower (Gahalaut et al., 2011; Vernant et al., 2014) than in other zones (Fig. 1), in particular to the west of Sikkim. This can be due to continental shortening being cushioned by the Shillong Plateau (SP) 150 km farther south (e.g. Bilham and England, 2001; Gahalaut et al., 2011). The present-day deformation pattern is constrained only by sparse GPS measurements in western Bhutan (Vernant et al., 2014) and a single estimate of Holocene uplift rate along the Topographic Frontal Thrust (TFT) in central Bhutan (Berthet et al., 2014). In central Nepal and Arunachal Pradesh (east Bhutan), Holocene slip rates along the MFT are about 21 ± 1.5 mm/yr (Lavé and Avouac, 2000) and 23 ± 6.2 mm/yr (Paul Burgess et al., 2012), respectively. The occurrence of the 1897 earthquake near the SP attests to the accommodation of the convergence in this region and has been proposed to increase the interval between great earthquakes in the Bhutan Himalaya (Bilham and England, 2001). Gahalaut et al. (2011) also proposed that the stress shadow caused by this earthquake may be responsible for the low seismicity rate currently observed in Bhutan. According with instrumental and historical records, Bhutan experienced no major earthquake in the past 200 years (Gahalaut et al., 2011).

2.2. Northeastern himalaya

The northeastern Himalaya is subdivided into four major tectonic units by different thrusts. From south to north (see Fig. 2): the *Outer Sub-Himalaya* (that lies between the MFT and the MBT), mainly consists of Neogene and Quaternary molasse sediments; the *Lesser Himalaya* (bounded by the MBT and MCT), consists in pre-Tertiary rocks that underlie the central Himalaya. While the MBT is clearly defined all along the southern margin of the Himalaya, the position of MCT is debated, particularly in the northeastern part.

The *Central Himalaya* is made by metamorphic and granitoid rocks and higher structural units to the north of MCT. In the *Trans-Axial Himalayas*, a tectonic contact being defined by the Tethyan/Trans-Axial Thrust or Indus Suture Thrust (IST) puts in contact Phanerozoic sediments and metasediments and the crystallines.

2.3. Eastern Himalaya Syntaxis

The Eastern Himalaya Syntaxis (“Assam syntaxis”) is a complex triple junction that joins the Indian and Eurasian plates with the northern end of the Burma platelet. The Himalayan arc shows a sharp turn of about 90° and meets the Indo-Burma ranges. The crustal deformation due to plate motions is particularly complex and this syntaxis zone is also the location of high stress concentrations. To the southeast and east of the Assam Syntaxis within east Burma and Yunnan (China), the relative motion between India and southeast Asia is dextral; to the west and north of the Syntaxis, within the Eastern Himalaya and southeast Tibet, the motion between India and Asia is convergent. The crustal thickness estimated in this region range from 50 to 60 km. This area was the place of the August 15, 1950 Assam earthquake (*Mw* 8.6): it is considered as the manifestation of the India-Asia convergence (Seeber et al., 1981). Armijo et al. (1989) supported the right-lateral strike slip solution on the Po Qu fault zone in southeast Tibet, which wraps around the Eastern Syntaxis and connects with the right-lateral strike-slip Sagaing fault zone.

2.4. Indo Burma ranges

The Indo-Burma ranges (IBR) is located in a complex tectonic zone with oblique subduction at its western boundary, a dextral transform fault (Sagaing fault) on the eastern boundary, the Mishmi thrust in the north, and the Andaman Spreading Ridge (ASR) to the south. The Burmese arc, NS oriented and 1100 km in length and 13–14 km in width, is convex westward. Different interpretations have been proposed through years about the evolution of the Burmese arc (Curray et al., 1979; Le Dain et al., 1984; Mitchell and McKerrow, 1975; Nandy, 1983; Tapponnier et al., 1982; Uyeda and Kanamori, 1979), but it is generally agreed that the IBR is a subduction zone characterized by high seismicity.

2.5. Shillong-Mikir Massif

The Shillong Plateau-Mikir Massif intraplate zone is a part of the Indian shield and moved to the east along the Dauki fault. The Shillong Plateau is located between the Himalayan arc to the north and the Burmese arc to the east; it was created by a “pop-up tectonics” in the Pliocene and it is bounded by active faults (Kayal et al., 2006; Saikia et al., 2017). To the south, the Plateau is limited by the ~320 km long E-W Dauki fault, that separates the Precambrian basement of the SP to the north and the thick Tertiary sediments of the Bengal basin to the south (Kayal, 2008; Sharma et al., 2017). The area between the SP and the Mikir hills is called the Kopili gap and they are separated through the NW-SE Kopili lineament (300–400 km long). The Kopili fault produced two large intraplate earthquakes, the damaging 1869 Cachar earthquake (*Mw* 7.4), and another one in 1943 (*Mw* 7.2). In January 2016 a strong intraplate earthquake of *Mw* 6.9 occurred at the southeast end of the Kopili fault in Manipur. To the west, the Plateau is bordered by the Dhubri fault, that generated the 1930 Dhubri earthquake (*Mw* 7.1) (epicenter at 25.8°N, 90.1°E and ~60 km depth). The northern boundary of the SP is not well constrained and different authors proposed different interpretation (Bilham and England, 2001; Kayal et al., 2006; Rajendran et al., 2004). For this study, according to Bilham and England

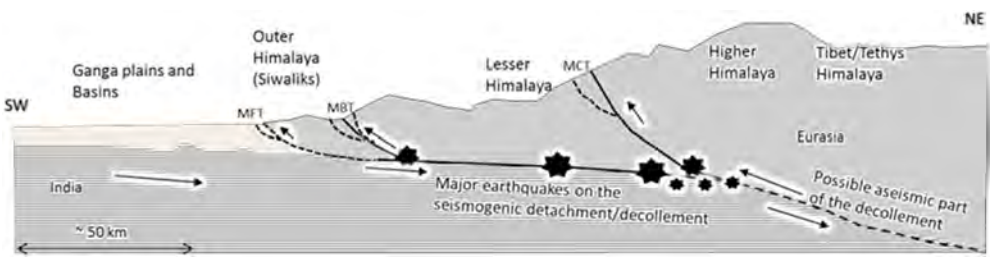

Fig. 2. Simple model of how the Indian continent underplates the Eurasian continent which gives rise to the Himalayas with the major faults Main Frontal Thrust (MFT), Main Boundary Thrust (MBT) and the Main Central Thrust (MCT) (Bungum et al., 2017).

(2001) based on GPS observations, we have considered that the SPis bounded by two reverse faults: the north dipping Dauki fault to the south and WNW-ESE trending south dipping Oldham fault at the boundary between the Plateau and the Brahmaputra valley. The Shillong Plateau-Mikir massif and Assam valley intraplate zone produced many large earthquakes, including the great Shillong earthquake, occurred in June 12th, 1897. It is one of the largest intra-plate earthquakes in the world, with a magnitude Ms 8.7 (revised *Mw* 8.1 by Bilham and England, 2001), and it was the first Indian earthquake for which instrumental records, recorded outside India, are available (Oldham, 1899). It caused widespread damages over the entire plateau and in NE India, causing 1542 casualties. Different interpretation (Baruah et al., 2016; Bilham and England, 2001; Imsong et al., 2016; Martin and Szeliga, 2010; Oldham, 1899) have been proposed to define the earthquake source. The scenarios based on either the Chedrang Fault or the Oldham Fault are more in line with the reported damage and shaking intensity reported from the 1897 event.

2.6. Assam valley

The Brahmaputra valley is divided into three parts: the eastern upper Assam valley, the central Brahmaputra valley and the western lower Assam valley. The Brahmaputra plain is stretched nearly 800 km in length with an average width of 110 km and runs NE-SW, and it is composed by Mesozoic to early Tertiary sediments that they increase the seismic hazard of the region. The Brahmaputra basin formed as a result of upliftment and subsidence of different blocks of Precambrian crystalline deposition. The Oligocene sequence in Assam shelf is represented by 600–1000 m thick sediments. The upper Assam valley is flat, about 100 km in width and 300 km in length and is NE-SW oriented (Saikia et al., 2017).

2.7. Bengal Basin

The Bengal basin is one of the largest basins of the world, with a thickness of up to ~15 km (Kayal, 2008). The Bengal geosyncline shrunk with time in consequence of the eastward subduction of the Indian plate below the Andaman-Burmese arc. Several stages have been observed: India collision with Eurasia, uplift and erosion of the Himalaya in the Tertiary-Quaternary, transport of the eroded materials by confluent Ganges and Brahmaputra rivers and deposition of the sediments in the newly formed Bengal geosyncline. Due to continued spreading of the Indian ocean floor, the above stages are still ongoing. An important tectonic feature is the Eocene Hinge Zone (500 km long, width varies from 25 km to 110 km), which separates the continental shelf to the west and the geosynclinal facies to the east. Curray et al. (1982) suggested that the Hinge line represents the boundary between the continental crust and the young oceanic crust that extends southwards into the Bay of Bengal, and it intersects the Dauki fault near 92°E. The Bengal basin has produced two large deeper (depth $\geq$ 20 km) intraplate earthquakes, one in 1918 (*Mw* 7.1) at the Sylhet fault, and the other in 1923 (*Mw* 7.0) at the junction of the Hinge zone and the Dauki fault.

3. Seismicity information

In order to completely represent source seismicity through a recurrence relation, the annual rate of earthquakes above a minimum magnitude is needed. There are basically two approaches to define activity rate of a given seismic source, either through the analysis of past seismicity from an earthquake catalogue or through structural geological data, such as faults information. The procedure to identify potential seismic sources in the studied region comprises an evaluation of the historical and recent instrumental seismicity data, emphasizing that these data are the primary empirical basis for conducting the seismic hazard analyses. Another information source is the evaluation of the tectonic history based on available geological data and information and finally a quantification of known seismicity and geology into model recurrence parameters used as basis for the PSHA.

3.1. Earthquake catalogues

An earthquake catalogue is an archive where all the past events are reported with information about magnitude, time and location, hypocentral depth and other source-specific information. The earthquake catalogues are, regrettably, inherently heterogeneous. From the early days of instrumental seismology at the beginning of the twentieth century, seismological networks have undergone many changes that are reflected in the database of earthquake records in use today. One of the challenges is related to the variety of scales used for recording earthquake magnitude. In 1964 the International Seismological Centre (ISC) catalogue shows a rapid increase in the reported earthquake globally. The ISC-GEM Extended catalogue, updated in July 2017, was used as one of the basic sources of information since it is based on reports from many international seismological networks and reporting agencies (Weatherill et al., 2016). The ISC-GEM Extended is a global homogenized catalogue (Weatherill et al., 2016) that represent seismicity in a common and comparable scale using the moment magnitude *Mw* scale. It contains data from 1900 through 2016, and in the region of interest the smallest magnitude reported is $Mw = 3.93$. Two other catalogues were taken into consideration: the Global Centroid Moment Tensor Catalogue (Global CMT) (Ekström et al., 2012) and the USGS earthquake catalogue (see Data Availability). In particular, the Global CMT catalogue database covers a period from January 1976 to December 2017 and it was used to evaluate the dominant rupture mechanisms of the area by means of ternary diagrams (Kaverina et al., 1996) (Fig. 3).

The USGS earthquake catalogue was used, together with the ISC-GEM Extended catalogue, for analyzing the hypocentral depth distribution of the past events and a statistical analysis was performed to understand how the ruptures are distributed along the depths.

There are many uncertainties that affect the catalogues. These uncertainties are basically related to the magnitudes, the precise hypocentral locations and the depths of the events (Gulia et al., 2012; Panzera et al., 2016). Another problem is linked to the short period of observation in comparison with the recurrence time of the large events. For example, the observation period of earthquake activity in the study area covers around 116 years and this means that the used earthquake information (reliably quantifiable) does not stretch longer back in history. Since the average return period of large earthquakes is assumed much

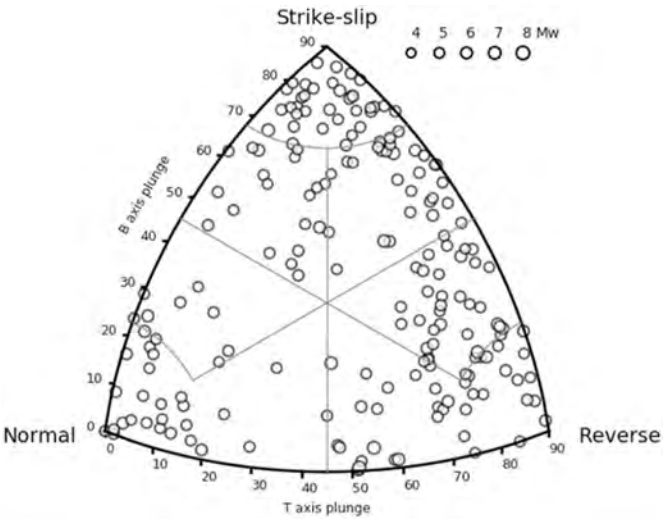

Fig. 3. The dominant rupture mechanisms for the entire study area are plotted in a ternary diagram, showing the main rupture kinematics (reverse, normal, strike-slip).

longer than 116 years, it becomes clear that the uncertainty of any hazard estimate is significant.

3.2. Declustering procedure

In order to perform a Poissonian analysis of the earthquakes in the catalogue, all the events must be independent from each other. Usually, after a larger earthquake, several events on a short time scale occur that are related to the previous one. These events, which are related to a parent event, are called aftershocks. Later, the time interval between earthquakes becomes longer. For what concerns the catalogue, it is important to perform the decluster procedure which removes the aftershock (and foreshock) events that are not allowed in the statistical analysis and violate the Poissonian assumption (Gardner and Knopoff, 1974; Hainzl et al., 2006; Taroni and Akinci, 2021; Zhuang et al., 2002). To remove the aftershocks and create a declustered ISC-GEM catalogue, many tests have been done to understand the sensitivity of the classical Gardner and Knopoff (1974) method. In this method, the earthquakes within certain time and distance windows of the mainshock, the size of which are defined by the mainshock magnitude, are considered dependent events and removed from the catalog. These windows are dependent only on the magnitude of the event and were derived for California earthquake. The Gardner and Knopoff (1974) algorithm resulted not suitable for the area investigated in this work because it was removing more than 40% of the total events, reducing the activity rates of the source zones. For this reason, a criterion based on a visual selection of the cluster events has been adopted. Different tests have been performed to evaluate the total number of events removed applying different time and distance windows. At the end, it has been decided to identify and remove the aftershocks from the catalogue listings if they satisfy the following assumptions:

- for events with magnitude equal or greater than 6.5, the distance considered for the decluster procedure was set to 70 km and the post-earthquake time set to two months;
- for main events with magnitude lower than 6.5, the distance was set to 50 km and the time set to one month.

Before the decluster procedure, the total number of the events were 4153 in the area between latitude 23°N to 30°N and longitude 85°E to 98°E; after applying the decluster method, the total events are 3050 (around 25% of the events have been removed).

3.3. Completeness of the catalogue

The magnitude completeness is the lowest magnitude above which 100% of the events in a space-time volume are detected; it is very important because it tells us from which years all the events above this threshold magnitude are detected and can be included in the statistical analysis. The magnitude completeness of an earthquake catalogue is a factor that profoundly affects the recurrence parameters, and it is a basic requirement for the processing of input data for seismic hazard analysis. After some tests with the Stepp (1971) algorithm, a manual procedure was selected for the characterization of the magnitude completeness based on the analysis of the obtained rates and the bins related to the magnitude are fairly homogeneous and growing with magnitude. The time-magnitude plot (Fig. 4) demonstrates that the ISC-GEM catalogue can be regarded as being reasonably complete for $M \geq 5.0$ only from 1965, because below $M < 5$ there is an evident irregularity in the distribution of events, that cannot be attributed to a problem of a simple incompleteness of the catalogue or to a real inhomogeneity of occurrences. From 1925 for $M \geq 5.5$ the figure again indicates complete recording. For $M \geq 6.5$, the catalogue has been considered complete from 1900. Finally, for $M \geq 7.5$ it's very difficult to say with certainty when it started to record; however, the recording start year has been estimated equal to 1850. It is worthy to note that the two major improvements in seismicity coverage occurred in the early 1960's (the WWSSN network) and around 2000.

3.4. Seismogenic faults

The modelling of all existing active faults as independent entities can be considered as the most accurate source model for seismic hazard assessment (Rivas-Medina et al., 2018; Stevens et al., 2020; Valentini et al., 2019). This idea is however quite idealistic, because many times earthquakes do not occur on pre-existing faults, and many faults in the sub-surface are simply not known in terms of size, geometry and potential. A more realistic view includes only a limited number of active faults that have the presumed highest seismic activity. The normal approach for mapping the faults is followed by different methods, for example field observation, morphological evidences, using aerial and satellite photos. Since it is extremely difficult to determine the correct

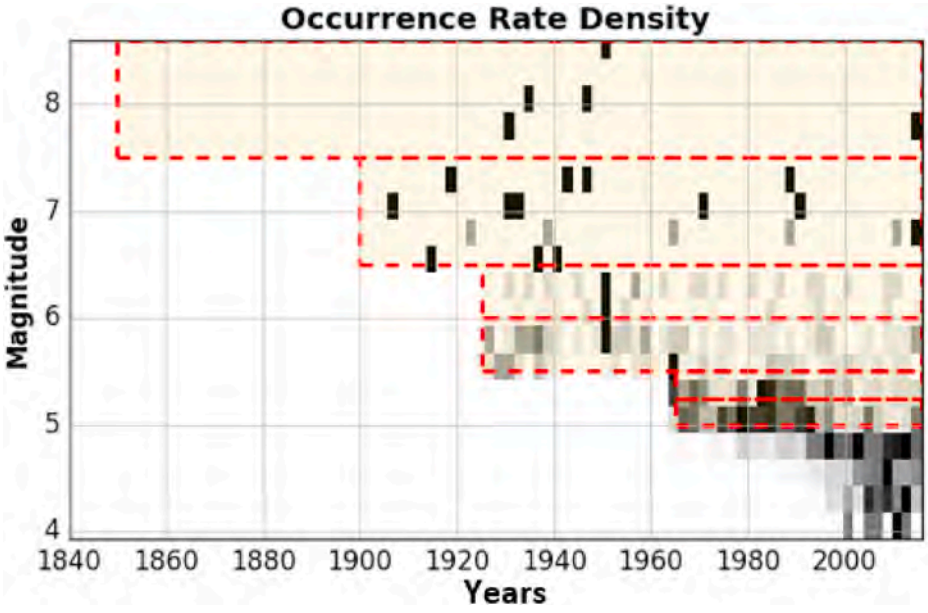

Fig. 4. Time-magnitude plot for the ISC-GEM catalogue for the identification of magnitude completeness thresholds.

fault traces and their precise position, simplified fault geometries have been adopted in this work. In this way, the computational efforts were reduced, without losing accuracy in the results. The faults information was taken from the Geological Survey of India (see Data Availability) and they were also supported by a careful literature research (Baruah et al., 2016; Bilham and England, 2001; Islam et al., 2011; Kayal, 2010). The following seismogenic faults (Fig. 5) have been considered: HFT (Himalayan Frontal Thrust), Yadong fault (strike-slip), Tista fault (strike-slip), Dhubri fault (left strike-slip), Kopili fault (right strike-slip), Oldham fault (reverse), Dauki fault (reverse fault). In section *2. Geology and Seismotectonics*, three superficial expressions of the MHT have been described: the HFT, the MBT and the MCT (Fig. 2). Since the MBT and MCT are possibly less important from the seismological point of view (there are no relevant events related to these thrust) than the underplating main thrust (MHT – detachment zone), in this work only the HFT and the MHT have been considered for the hazard calculation. In Fig. 5 only the HFT is represented because the MHT starts at about 17 km deep until ~50 km. The HFT is considered as the principal superficial expression of the MHT. The most important parameter for crustal deformation is the slip rate (in units of mm/yr); the slip rate of a fault is the speed with which one side of the fault moves with respect to the other. Slip rates are today most often estimated from GPS measurements, but nevertheless often remain uncertain. Moreover, it has to be considered that not all the slip rates value recorded by GPS can generate future earthquakes, since much of this slip is accommodated and converted in deformation (e. g. aseismic creep; Murray et al., 2014; Thatcher and Pollitz, 2008). The percentage of the slip rates that takes account for future earthquakes is called seismic coupling coefficient and is usually a value between the 30% and 50% of the registered data. When the slip rates are available, algorithms based on such estimates are considered to represent the most viable alternative provided that the derived activity is always assessed in terms of the equivalent moment release. Moreover, such approach assumes that the slip rate observed can be considered constant back in past times. When the slip rates are not available, the earthquake activity on a fault has to be assessed by assigning to the fault a certain proportion of the seismic activity which is assessed for the region containing the fault.

Regarding the faults, the main uncertainties are related to the correct fault traces and their locations, the slip rates values, the dip and depth of the faults. A way to overcome the problem of the correct fault traces and their locations can be comparing field data, morphological evidences, aerial and satellite images and try to define a simplified geometry. The variations in geometry (both strike and dip and possible listricity) can be accommodated by assigning the different geometries with appropriate weights in the model, and in this way consider several plausible alternatives. The solution to overcome the uncertainties related to the slip rate could be do different tests to extract the recurrence parameters changing each time the value of the slip rate. In this way, a sort of balance between the recurrence parameters used and the percentage of the slip rate used can be created for building a model much credible and realistic as possible.

4. The seismic source model

The hazard calculation for this work is mainly performed using two types of sources: the area sources and finite faults.

4.1. Area sources

The earthquake catalogue is used to build the spatial and temporal occurrence model that can be used as input for seismic hazard assessment, providing essentially a prediction model for a number of expected events at different magnitude levels and in different source regions.

4.1.1. Seismic zonation, maximum magnitude, depth distribution and moment tensors

The area sources can be described by areal regions in which earthquakes may occur anywhere and randomly within the defined zone and these zones are assumed to have uniform source properties in both time and space. The zonation has the purpose of dividing the seismicity into distinct source zones, and subsequently evaluating the seismic potential in each zone based on past seismicity. This is clearly a simplification with respect to the more continuous seismicity distribution. A main goal applied in a zonation process is to represent the seismicity and the tectonics as balanced as possible. In making the zonation, the basic principles were used as guidelines: each zone should be large enough to

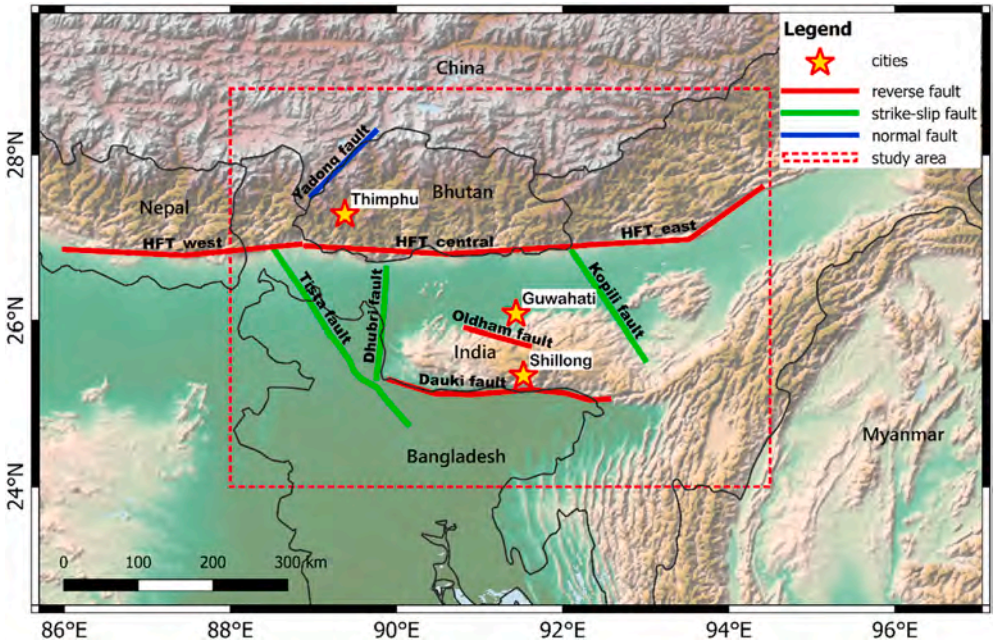

Fig. 5. The study area for hazard calculation is marked by a black dashed square (24–28.8° N to 88–94.5° E); and in the figure the main seismogenic faults of the area are shown as modelled with a simplified geometry: in red the reverse faults, in green the strike-slip faults, in blue the normal fault. (For interpretation of the references to colour in this figure legend, the reader is referred to the Web version of this article.)

allow for a reasonably stable assessment of recurrence parameters and a homogeneous source zone should encompass regions of supposedly uniform seismic potential and seismotectonic characteristics; the zones should cover all areas where the seismicity could have some influence on the seismic hazard, which normally means 200–300 km around the site, depending on activity level (this because also events that occur outside the study area can be relevant for the hazard level of the region of interest); the zonation should, if required, allow for possible regional differences in seismogenic conditions (focal depths, maximum magnitudes and faulting mechanisms); the zonation should be consistent with the regional geology and tectonics.

Based on the above tectonic knowledge, structural geology, main active faults and earthquake distribution the division into ten distinct seismic zones was made (Fig. 6). The division was based also on the data processing of the whole catalogue regarding the seismicity, depth and the previous studies (Baruah et al., 2016; Bilham and England, 2001; Islam et al., 2011; Kayal, 2010). The maximum magnitudes (Mmax) were defined, using the ISC-GEM Extended catalogue, for each of the zones defined through a combination of the observed maximum magnitude for each zone and the evaluated tectonic potential, where a simple and commonly applied rule is that Mmax should be set to about 0.5 magnitude units above the largest value.

- Zone 1 represents largely the Burmese Arc subduction zone. It is a very active seismic region and the Mmax is been fixed equal to 8.2. In this zone about half of the events show a reverse kinematic, and the other half a strike-slip mechanism;
- Zone 2 corresponds to the Bengal Basin with a Mmax equals to 7.7. In this case, there are less events but they show both reverse and strike-slip kinematics;
- Zone 3 or the Shillong area, where the 1930 Dhubri earthquake occurred with a Mw 7.1, and in this case the Mmax used is 7.6;
- Zone 4, called the Mikir Massif region, shows a strike-slip behaviour and during 1943, the Kopili earthquake was recorded with a Mw 7.2. So the Mmax used for the model is equal to 7.7;
- Zone 5, named also Eastern Himalaya Syntaxis, is note for the great 1950 Assam earthquake with a Mw 8.6. In this zone, the magnitude of the largest earthquake recorded is above 8.5, that is a value for which an increase of 0.5 would lead to a Mmax that should be not realistic. In this case, the catalogue has registered an event that is probably very close to the maximum awaited. For this reason, the model Mmax has been put equal to observed Mmax 8.6;
- Zone 6, called here India region, is represented by a low seismicity distribution and the Mmax is 7.3;
- Zone 7 or Nepal region, is marked by the west part of the Himalayan Frontal Thrust. The 1934 earthquake recorded a Mw 8 so the Mmax used is 8.5. In the area, half of the events indicate a reverse kinematic, and the other half is marked by both normal and strike-slip mechanisms;
- Zone 8, called Bhutan region, shows a reverse mechanism confirmed by the central part of the HFT. In this case the Mmax used is 7.0;
- Zone 9, named Arunachal Pradesh, is characterized by a reverse mechanism and through the east part of the HFT. The Mmax is 7.8;
- Zone 10 comprises the China area and shows a low seismicity distribution (Mmax used 6.5) with a normal kinematic.

The hypocentral depth distribution has been analyzed using two different catalogues: the ISC-GEM Extended and the USGS earthquake catalogues (Fig. 7).

4.1.2. *Quantification of the earthquake recurrence*

In each source zone, the temporal occurrence of events with increasing magnitude is assumed to follow a power-law behaviour, which we model using a double truncated Gutenberg-Richter recurrence relation (or magnitude-frequency distribution, MFD) (Gutenberg and Richter, 1956). Lower truncation is arbitrarily assigned to *Mw* 4.5 (lowest magnitude threshold considered capable of generating damage) for all zones. Upper truncation is defined as the magnitude of the largest earthquake assumed possible for an area (explained in the previous section and in Table 2). The ISG-GEM Extended catalogue was used to compute the *b*-value. Since the *b*-value heavily affects the hazard calculation, and the uncertainty on *b* in some zones is very high, due to the small number of events available in each zone, we decided to set this value equal to the *b*-value obtained for the total area. In a first round, the *b*-value has been computed for the total area using the linear regression method, and then the rates are obtained for each zone by using the fixed *b*-value (Table 2).

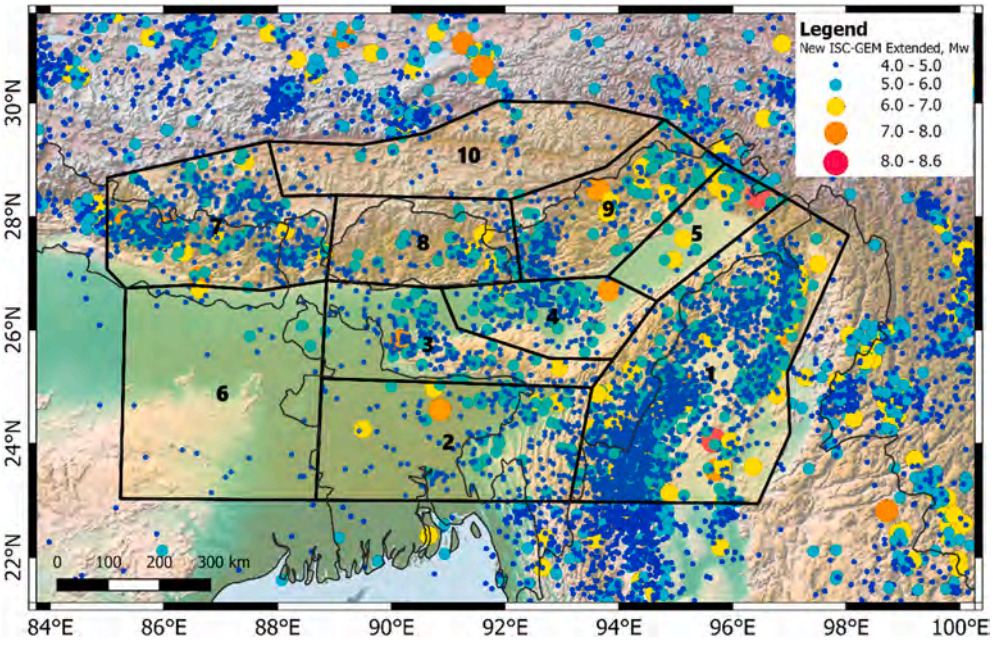

Fig. 6. The zonation of the study area, taking into consideration the earthquakes distribution, the main active faults and the geological framework of the area.

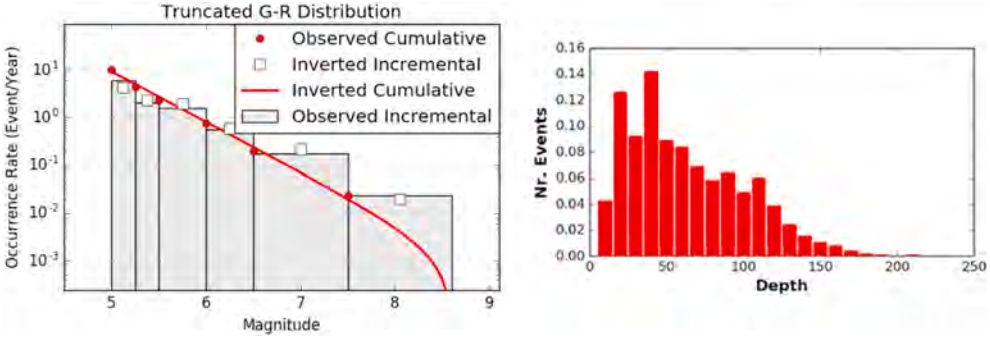

Fig. 7. On the left, the magnitude-frequency distributions and recurrence regressions for the determination of the recurrence values for the entire study area. White squares and red dots are respectively the observed incremental and cumulative occurrence rates, while the grey histogram and the red line represent the incremental and cumulative rates from the inverted Gutenberg–Richter relation. It must be noted that the width of noncumulative magnitude bins is not uniform, as this is not a requirement of the fitting method. On the right, the hypocentral depth distribution is shown for the whole study area with the filter for depths 10 and 33 km. (For interpretation of the references to colour in this figure legend, the reader is referred to the Web version of this article.)

Table 1
In the table, the fault geometries are summarized (rectangular fault planes), the original length, the length of each fault after the segmentation procedure and the aspect ratio for the segmented parts.

Fault	Width	Original Length (km)	Number of segments	Length after the segments (km)	Aspect ratio	Slip rate from GPS data (mm/yr)	Slip rate used (mm/yr)
Dauki	40	300	3	100	2.5	5.00	2.00
Dhubri	25	165	3	55	2.2	0.80	0.32
Kopili	50	200	2	100	2.0	2.50	1.00
Oldham	40	88	1	88	2.2	5.00	2.00
Tista	40	320	4	80	2.0	1.50	0.60
Yadong	25	125	2	62.5	2.5	0.50	0.20
HFT-central	70	350	2	175	2.5	17.00	6.80
HFT-east	60	240	2	120	2.0	21.20	8.48
HFT-west	60	300	2	150	2.5	19.40	7.76

4.2. Fault sources

The main seismogenic faults of the area were considered and they have been treated and modelled in a simplified way to perform the hazard calculation (Fig. 5). The information about faults focal mechanisms are extracted from the literature review (Baruah et al., 2016; Bilham and England, 2001; Islam et al., 2011; Kayal, 2010). In most cases the dip and the depth information are not available, and the values used refer to extrapolated data from figures or from a geological interpretation. For a long fault or fault system, some segmentation is usually needed when evaluating the potential seismicity, or the recurrence characteristics. Since it is not realistic that a fault ruptures along its entire length, faults and fault systems are segmented when evaluating their seismic potential in order to avoid unrealistically large magnitude earthquakes. If the fault is modelled with the real length (without segmentation), the *a*-value and the maximum magnitude would be unrealistically high, corresponding to the fault length. For this reason, knowing the fault width factor, the aspect ratio was fixed to extract the segments fault length. The aspect ratio is given by the ratio between the fault length and the fault width factor. The details of the segmented model faults are provided in Table 1. In this work, the data about the slip rates is derived from GPS measurements (Barman et al., 2017; Bilham and England, 2001; De and Kayal, 2003; Diehl et al., 2017; England and Bilham, 2015; Goswami, 2005; Hauck et al., 1998; Hetényi et al., 2016; Kayal et al., 2006; Le Roux-Mallouf et al., 2015; Marechal et al., 2016; Nandy, 2001; Stevens et al., 2020; Stevens and Avouac, 2015; Velasco et al., 2007; Vernant et al., 2014; Yin, 2006). However, many times the value recorded by GPS is converted directly without considering that not all the slip rates can generate future earthquakes, but much of this slip is accommodated and converted in deformation (Murray et al., 2014; Thatcher and Pollitz, 2008). After different sensitivity tests, the 40% of the GPS recorded slip rate of each fault has been used (Table 1).

The estimation of activity rates (*N*-values) involves the seismic moment, M_0, the rigidity or shear modulus, μ, the total average displacement (or slip) across the fault, D, the annual slip or slip rate, S, and the rupture area, $A = LW$, where L is fault length and W is fault width. Knowing the slip rate and the rupture length of the faults, we extracted the *a*-value (keeping fixed the *b*-value at 1.05, like the area sources; see Table 3) using an average model based on Anderson and Luco (1983) (Eq. (1), Eq. (2), Eq. (3)) and Youngs and Coppersmith (1985) (Eq. (4)) relations (Bungum, 2007).

Anderson and Luco (1983) proposed the following relationships for the determination of the number of earthquakes N above the lower bound magnitude (around 4–5) on a fault:

$$N_1(M) = \left(\left(\overline{d} - \overline{b}\right) \Big/ \overline{d}\right)(S/\beta)e^{\overline{b}(M_{max}-M)}e^{-\left((\overline{d}/2)M_{max}\right)} \quad \text{Eq. 1}$$

$$N_2(M) = \left(\left(\overline{d} - \overline{b}\right) \Big/ \overline{b}\right)(S/\beta)\left[e^{\overline{b}(M_{max}-M)} - 1\right]e^{-\left((\overline{d}/2)M_{max}\right)} \quad \text{Eq. 2}$$

$$N_3(M) = \left(\overline{d}\left(\overline{d} - \overline{b}\right) \Big/ \overline{b}\right)(S/\beta)\left\{1 \Big/ \overline{b}\left[e^{\overline{b}(M_{max}-M)} - 1\right] - (M_{max} - M)\right\}e^{-\left((\overline{d}/2)M_{max}\right)} \quad \text{Eq. 3}$$

Table 2
All the parameters related to the area sources necessary for the hazard calculation. The column "Id" is relative to the identificative number of each area; the "Depth range" put in relation the minimum and the maximum depth where the events can generated; the "Hypocentral depth" is expressed by a statistical analysis for a specified depth; the "M range" is relative to the Mmin and Mmax used; the a and b-values of the Gutenberg-Richter recurrence law (obtained from the catalogue); and finally the "Focal mechanisms" expressed in terms of probability, specifying the most representative strike, dip and rake of the area.

Id	Name	Depth range (km)	Aspect ratio	Hypocentral depth (km) = probability	M range	*a*-value	*b*-value	Focal mechanisms (probability - strike,dip,rake)
1	Burmese Arc	0–150	2.0	17.5 = 0.15 52.5 = 0.30 87.5 = 0.35 122.5 = 0.20	4.5–8.2	5.89	1.05	0.25–0,90,180 0.25–290,90,0 0.25–35,45,90 0.25–35,60,90
2	Bangal basin	0–80	2.0	10 = 0.18 30 = 0.44 50 = 0.28 70 = 0.10	4.5–7.7	5.06	1.05	0.25–90,45,90 0.25–270,45,90 0.25–45,70,45 0.25–45,90,0
3	Shillong	0–80	2.0	10 = 0.26 30 = 0.44 50 = 0.24 70 = 0.06	4.5–7.6	4.73	1.05	0.50–330,90,180 0.50–330,60,45
4	Mikir Massif	0–80	2.0	10 = 0.17 30 = 0.28 50 = 0.46 70 = 0.09	4.5–7.7	4.81	1.05	0.50–330,90,180 0.50–330,60,45
5	Eastern Himalaya Syntaxis	0–80	2.0	10 = 0.31 30 = 0.52 50 = 0.14 70 = 0.03	4.5–8.6	4.87	1.05	0.40–225,30,90 0.40–315,30,90 0.20–50,50,90
6	India region	0–80	2.0	10 = 0.20 30 = 0.48 50 = 0.16 70 = 0.16	4.5–7.3	4.47	1.05	1.00–0, 90,180
7	Nepal (HFT-west)	0–80	2.0	10 = 0.32 30 = 0.31 50 = 0.21 70 = 0.16	4.5–8.5	5.25	1.05	0.20–320,90,180 0.25–270,30,90 0.25–270,10,90 0.30–45,45,-90
8	Bhutan (HFT-central)	0–80	2.0	10 = 0.43 30 = 0.30 50 = 0.18 70 = 0.09	4.5–7.0	4.85	1.05	0.50–270,30,90 0.50–270,10,90
9	Arunachal Pradesh (HFT-east)	0–80	2.0	10 = 0.33 30 = 0.40 50 = 0.19 70 = 0.08	4.5–7.8	4.99	1.05	0.50–225,30,90 0.50–225,10,90
10	China	0–80	2.0	10 = 0.38 30 = 0.34 50 = 0.18 70 = 0.10	4.5–6.5	4.31	1.05	1.00–70,40,-90

where $\overline{b} = b(\ln(10))$, $\overline{d} = d(\ln(10))$, $\beta = \sqrt{(\alpha M_0(0)/(\mu W)}$ and $M_0(0)$ is the seismic moment for $M_s = 0$. The parameter d is the magnitude scaling coefficient in the log-linear relation between moment and magnitude, of the form $\log M_0 = c - dM$ (Kanamori and Anderson, 1975).

In addition to these three models, also Youngs and Coppersmith (1985) relation has been considered:

$$N_4\left(m^0\right) = \frac{\mu A_f S(d-b)\left[1 - e^{-\beta\left(m^u - m^0\right)}\right]}{bM_0^u e^{-\beta(m^u - m^0)}} \quad \text{Eq. 4}$$

where m^0 is some arbitrary reference magnitude, $m = b(\ln(10))$, $A_f = LW$ is fault area and m^u is an upper bound magnitude.

The maximum magnitude of the faults is essentially assessed from the segmented fault length (Table 3). The Wells and Coppersmith (1994) magnitude-scaling relationship was used, that is based on a global database of historical earthquake ruptures and it works for shallow earthquakes in active tectonic regions.

5. Ground motion model

During the last three decades, more than 500 different Ground Motion Prediction Equations (GMPEs) have been produced around the world (Douglas, 2019), and new equations (or the update version of existing ones) are periodically released. However, despite the presence of large methodological similarities between GMPEs, the predicted ground motion proves to be highly variable. A careful evaluation should be performed when selecting the most suitable GMPEs for a given study region. There are few relations available that have been developed specifically for the Himalayan region and hardly for any region with reasonably similar tectonics. However, the approach that is used for selecting GMPEs for the study area is to use empirical relations based on observed data from other similar active regions. The proper calibration of such relations is difficult, leading to considerable uncertainties in the prediction of ground motions, and from the largest earthquakes. In a first round, eleven GMPEs were selected as possible candidates, covering three different tectonic contexts: active shallow crust (ASC), stable continental crust (SCC), and subduction zone (SZ). These GMPEs have been tested and compared with their hazard curves and response spectra and only some of these have been considered suitable for the study area (Fig. 8), taking into consideration some information get from literature and the magnitude range of operation.

While the aleatory component of the model uncertainty is generally taken into account through the hazard integral, the epistemic component, which is related to the available level of knowledge and the adopted initial assumptions and simplifications, can be quantified by using a logic-tree approach. The need of a logic-tree scheme is also due to the fact that there is no GMPE calibrated on local settings, since few

Table 3
The necessary parameters to model the faults. The columns "Rake" and "Dip" are related to the faults geometry; the "Upper-Lower seismogenic depth" put in relation the minimum and the maximum depth where the events can generated; the "Hypocentral depth" is expressed by a statistical analysis for a specified depth; the "M range" is relative to the Mmin and Mmax used; the a and b-values of the Gutenberg-Richter recurrence law (obtained from the slip rates).

Name	Rake	Dip	Upper-Lower seismogenic depth (km)	M range	*a*-value	*b*-value
Dauki (reverse)	90	50	0–40	4.5–7.75	4.69	1.05
Dhubri (strike-slip)	0	90	0–35	4.5–7.29	3.64	1.05
Kopili (strike-slip)	180	60	0–50	4.5–7.91	4.47	1.05
Oldham (reverse)	90	57	0–40	4.5–7.69	4.67	1.05
Tista (strike-slip)	180	90	0–40	4.5–7.69	4.14	1.05
Yadong (normal)	−90	60	0–20	4.5–7.33	3.46	1.05
HFT-central (reverse)	90	/	0–48	4.5–8.24	5.49	1.05
HFT-east (reverse)	90	/	0–47	4.5–8.01	5.48	1.05
HFT-west (reverse)	90	/	0–47	4.5–8.11	5.47	1.05

data of the study region are available. The current logic-tree model is using two separate branching levels for active shallow crust and subduction zone regions (Fig. 9).

For the active shallow crust region, two GMPEs (Boore et al., 2014; Boore and Atkinson, 2008) were used with equal weights in the logic-tree calculation (0.5 each). For the subduction zone, it was decided to use a logic-tree based on Boore and Atkinson (2008) with weight 0.4 and Atkinson and Boore (2003) with weight 0.6. For the subduction zone, it was decided to use Atkinson and Boore (2003) relation, specifically developed for this type of areas, in combination with Boore and Atkinson (2008) relation, since there is a zone component which can be modelled as active. All the area sources and the faults have been modelled like ASC, except for the Burmese Arc zone that is modelled like SZ.

6. Results

Individual PSHA results from each seismicity model (area sources, fault model and hybrid model) are presented and evaluated with *OpenQuake* (OQ) software (Version 2.7); it is an open source and community-driven seismic hazard and risk calculation software developed by the Global Earthquake Model (GEM) foundation. The magnitude-frequency distribution chosen is a double truncated Gutenberg-Richter distribution. This is described by means of Mmin and Mmax and by the *a* and *b*-values of the Gutenberg-Richter relationship. The magnitude-scaling relationship adopted is the Wells and Coppersmith, 1944 (*WC1944*) for shallow earthquakes in active tectonic regions and it is based on a global database of historical earthquake ruptures. The seismic hazard calculations have been carried out by performing hazard computations at a grid interval of 15 km, covering the entire study region delimited by latitude 24°-28.8°N and longitude 88°-94.5°E. Peak Ground Acceleration (PGA) and Spectral Acceleration (Sa) values for six different periods (from 0.05 to 2.0 s) have been evaluated at bedrock level (Vs30 equal to 800 m/s) corresponding to a probability of exceedance (POE) of 10% in 50 years. This exceedance value corresponds to return periods of 475 year. For each grid point, all the sources within a radius of 200 km were considered for the evaluation of PGA and Sa values. The hazard results are presented by hazard maps for the study area, and all ground-motion exceedance values are computed through hazard curves and mean and quantile (0.15,0.5 and 0.85) Uniform Hazard Spectra (UHS) for three important cities:

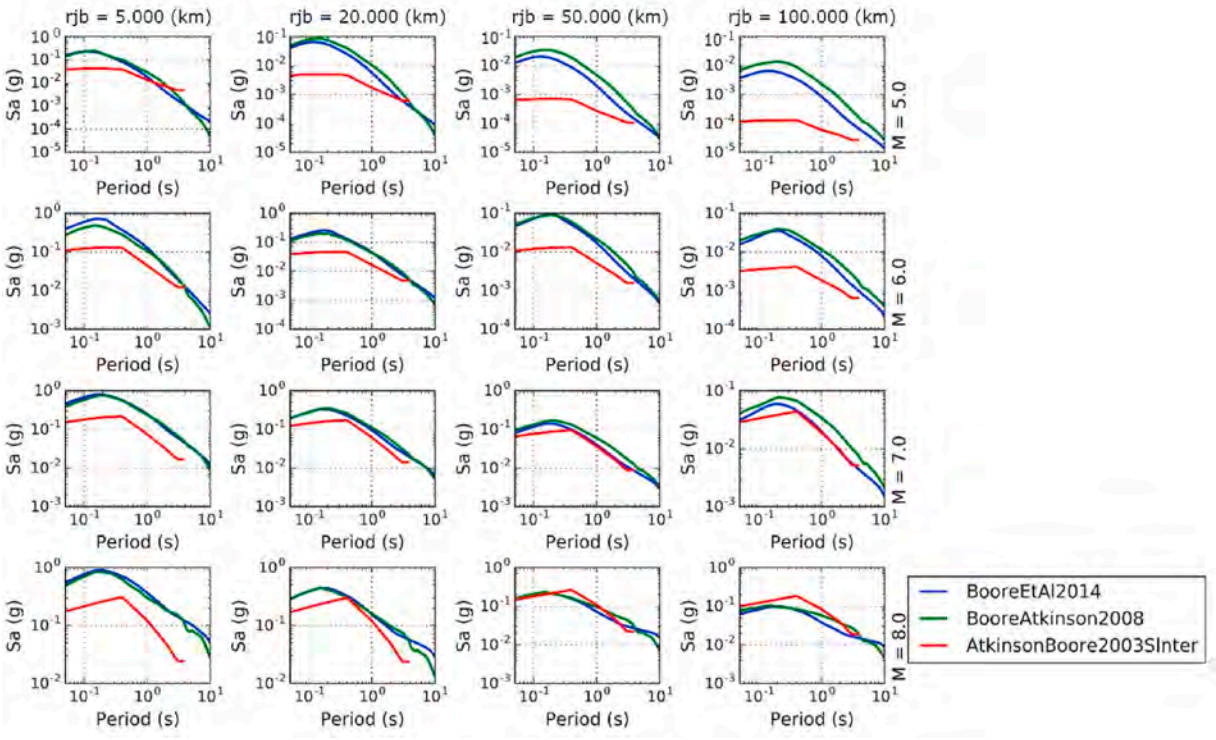

Fig. 8. Comparison between Boore et al. (2014), Boore and Atkinson (2008) and Atkinson and Boore (2003) models used in the logic-tree scheme; the response spectra are shown for different magnitudes (5.0, 6.0, 7.0, 8.0) and for different distances (5, 20, 50, 100 km).

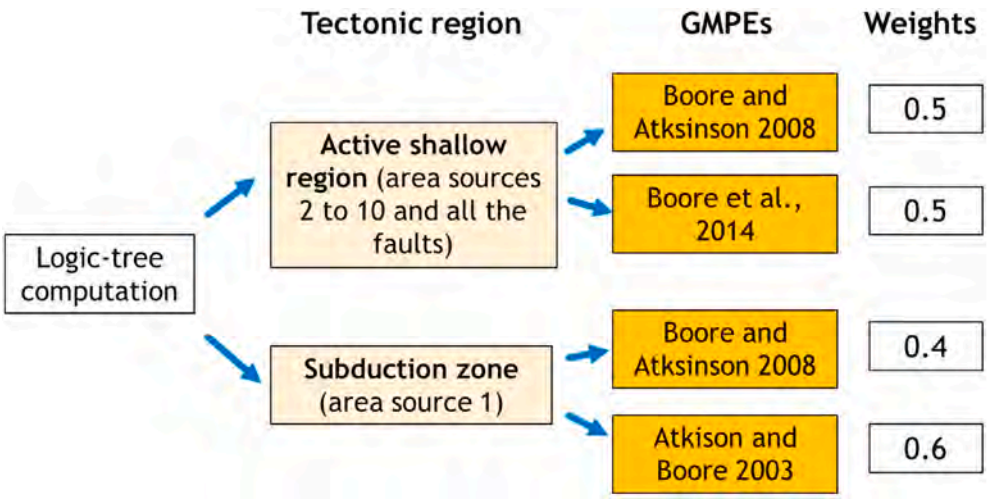

Fig. 9. Logic-tree model using two separate branching levels for active shallow crust and subduction zone regions.

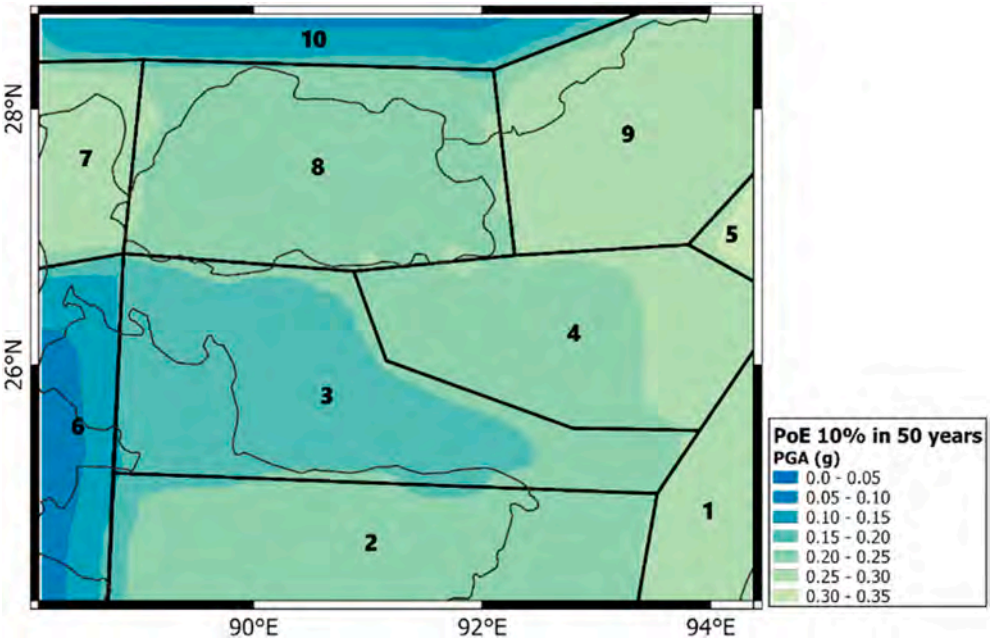

Fig. 10. The hazard map including only the area sources. The hazard map is shown in PGA using the g scale for the ground motion. The probability of exceedance is 10% in 50 years, corresponding to 475 years return periods.

Thimphu (27.28°N, 89.38°E), Guwahati (26.08°N, 91.44°E) and Shillong (25.34°N, 91.53°E). For each model, an example is shown for Shillong city and at the end in the hybrid model the results are plotted for all the three cities.

6.1. Calculation with only area sources

In a first calculation, only the area sources have been considered, using the recurrence model extracted from the seismic catalogue; all the areas have been modelled with the parameters listed in Table 2.

Fig. 10 shows the hazard map for the study area. The area sources are used to describe the seismicity occurring over a wide area where the identification and characterization of a single fault is difficult; in this case, the seismicity is equally distributed in each point of each area. The maximum PGA calculated is 0.35 g and it is shown in the two areas called "Eastern Himalayan Syntaxis" and "Burmese arc". In Fig. 11, the hazard curve and the UHS (fixing the annual rate of exceedance like 10% in 50 years) are shown for Shillong city). Looking at the UHS, the maximum mean SA value is recorded at 0.1 s and it is equal to 0.45 g.

6.2. Calculation with only faults

A second calculation has been carried out with only the faults with derivation of the recurrence model data from GPS data. In this model, all the faults (except to the Himalayan Thrust) are modelled like simple fault: the simple adjective relates to the geometry description of the source which is obtained by projecting the fault trace along a characteristic dip direction (by extending the fault up to the surface maintaining the fault dip). The Himalayan Frontal Thrust is modelled like a complex fault: the complex adjective refers to the fact that the fault can be realized as a union of planes with different dips. Complex faults are generally used to model intraplate megathrust faults such as the big subduction structures active in the Pacific, but also to create listric fault sources with a realistic geometry. The first part of the HFT, that reaches the surface, has been built with 25° dip (40 km width), the second one with 10° dip (60–70 km width) and the last part that arrives at 50 km

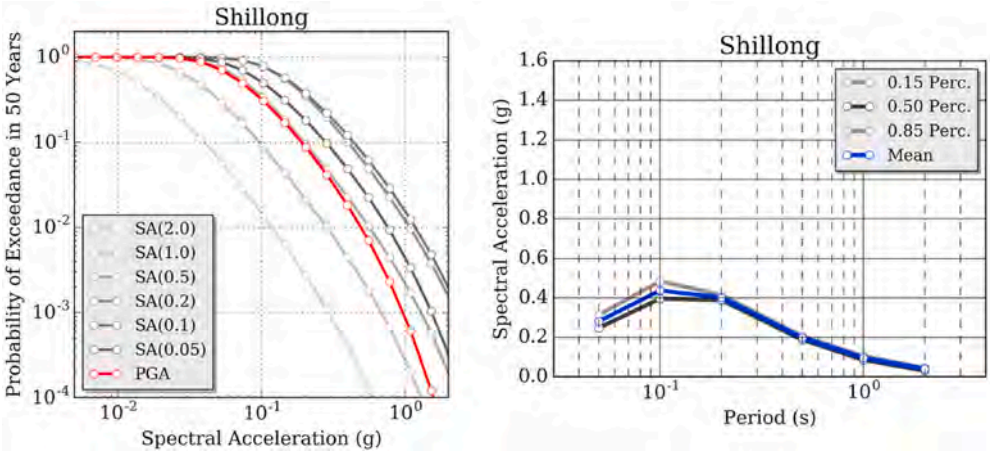

Fig. 11. Calculation with only the area sources: on the left, the mean hazard curves computed for a range of spectral periods, including PGA; on the right, mean and quantile UHS for Shillong city for 10% POE in 50 years.

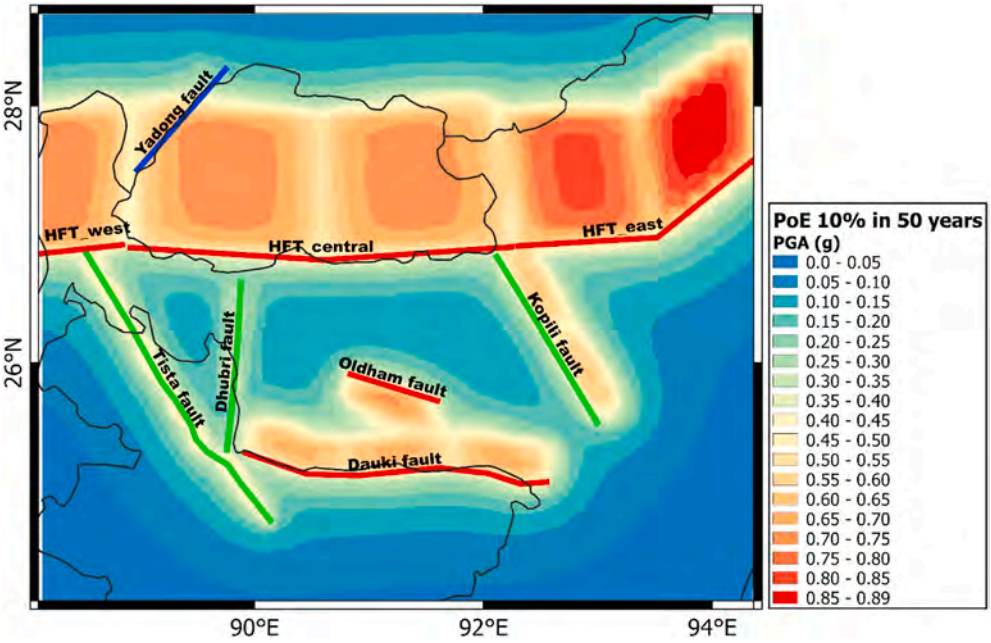

Fig. 12. The hazard map including only the faults. The hazard map is shown in PGA using the g scale for the ground motion. The probability of exceedance is 10% in 50 years, corresponding to 475 years return periods.

deep with 30° dip (40 km width) (Zhang et al., 2016). In the model with only the faults, both simple and complex faults have been considered and the parameters needed for the calculation are listed in Table 3.

Fig. 12 shows the hazard map for the area, and, as it can be observed, the Himalayan thrust affects most the results. The maximum PGA calculated is 0.89 g and it is recorded in the northeast part of the Himalayan thrust. This value is particularly high, and it could be attributed to the way the thrust is modelled. Looking at the UHS for Shillong in Fig. 13, the maximum mean SA recorded is correspondent to 1.45 g at 0.1 s. The SA is very high due to the proximity of Shillong city near the Dauki and Oldham faults.

6.3. Calculation with hybrid model

The purpose of this calculation is to combine the seismic potential of both types of sources that is derived from different data: for the zones, the recurrence model is estimated from the seismic catalogue; and for the faults, it is deduced from fault geometries and slip rate estimates derived from GPS measurements. However, the problem of using a model which combines zones and faults is establishing the distribution of seismic potential between them, considering that they are derived from different data sources. The problem is that a part of the events contained in the catalogue are linked to faults and they were already included in the seismic potential of the faults derived from slip rate estimates. If all events are assigned to the zones, the events related to the faults would be double-counted, and at the end the total seismic potential can be overestimated. Finding a solution to distribute the seismic potential appropriately is not easy. An approach to avoid the double-counting could be to fix the magnitude at a certain value to separate the seismic potential to the areas or to the faults. In this work, the magnitude was fixed at 6.5 to distinguish the different sources for the seismic potential (Fig. 14): for $M < 6.5$, the seismic potential is attributed to the area sources and for $M \geq 6.5$ the seismic potential is related to the faults. In this way, the big events are related the faults and the low grade of seismicity to the area sources like basic seismicity. Fig. 15 shows, as expected, how the Himalayan thrust dominates the seismic

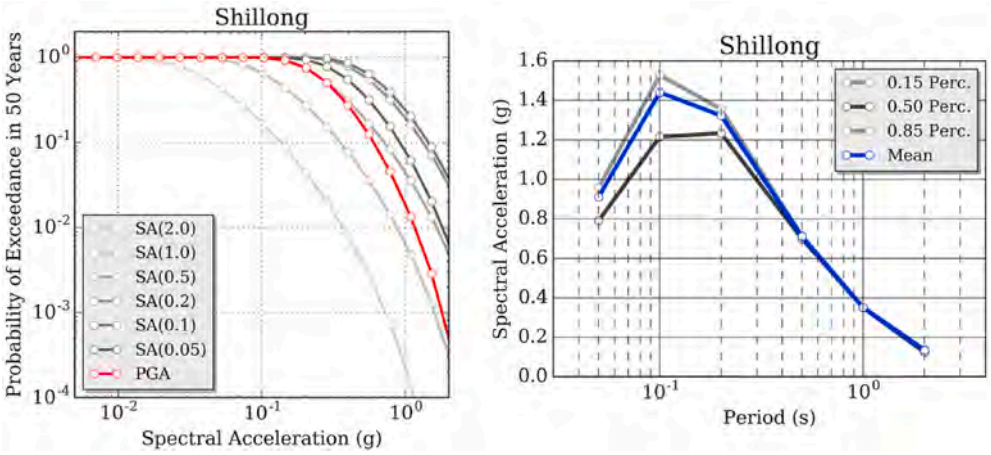

Fig. 13. Calculation with only the faults: on the left, the mean hazard curves computed for a range of spectral periods, including PGA; on the right, mean and quantile UHS for Shillong city for 10% POE in 50 years.

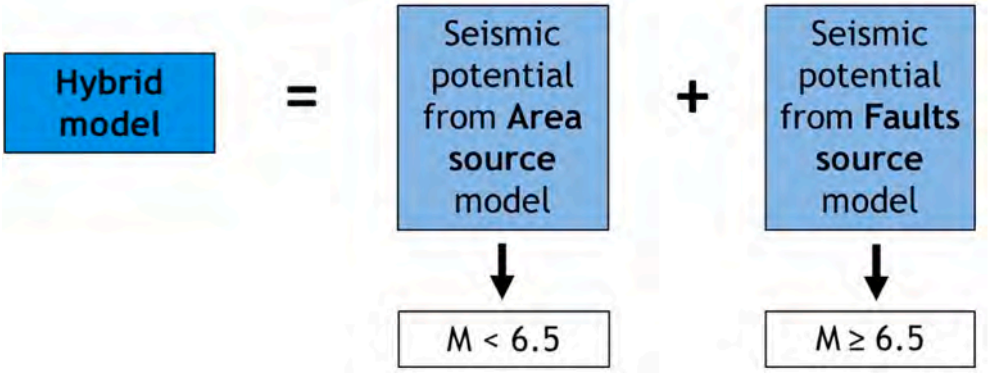

Fig. 14. The diagram shows how the seismic potential form the area and faults sources models are combined together into the hybrid model. To avoid the double-counting, the magnitude is fixed at 6.5 to distinguish the different sources: for $M < 6.5$, the seismic potential is attributed to the area sources and for $M \geq 6.5$ the seismic potential is related to the faults.

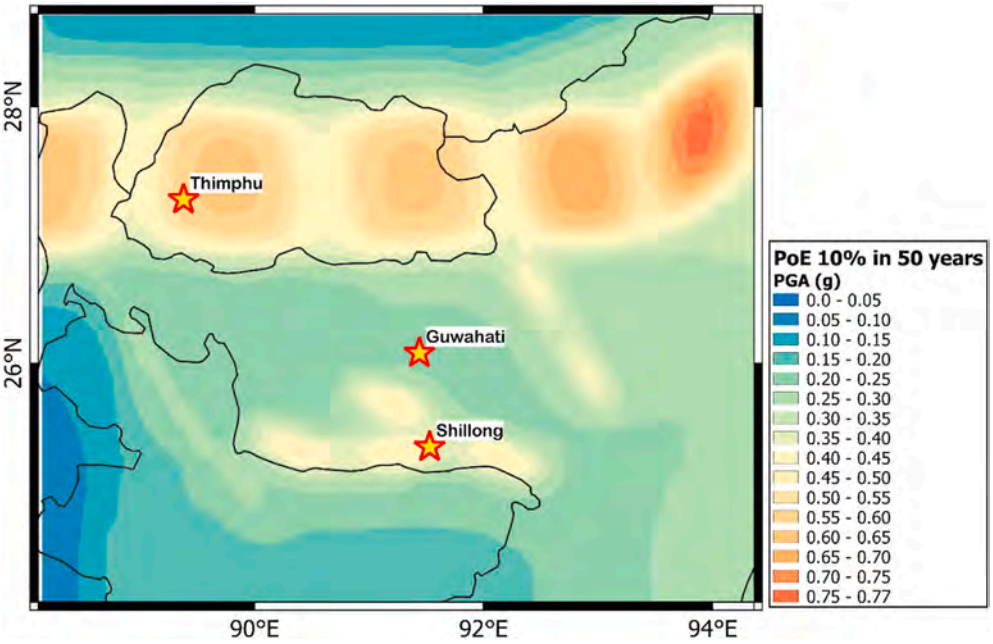

Fig. 15. The seismic hazard results including both the two types of sources, zones and faults, in the study area. The hazard map is shown in PGA using the g scale for the ground motion. The probability of exceedance is 10% in 50 years, corresponding to 475 years return periods.

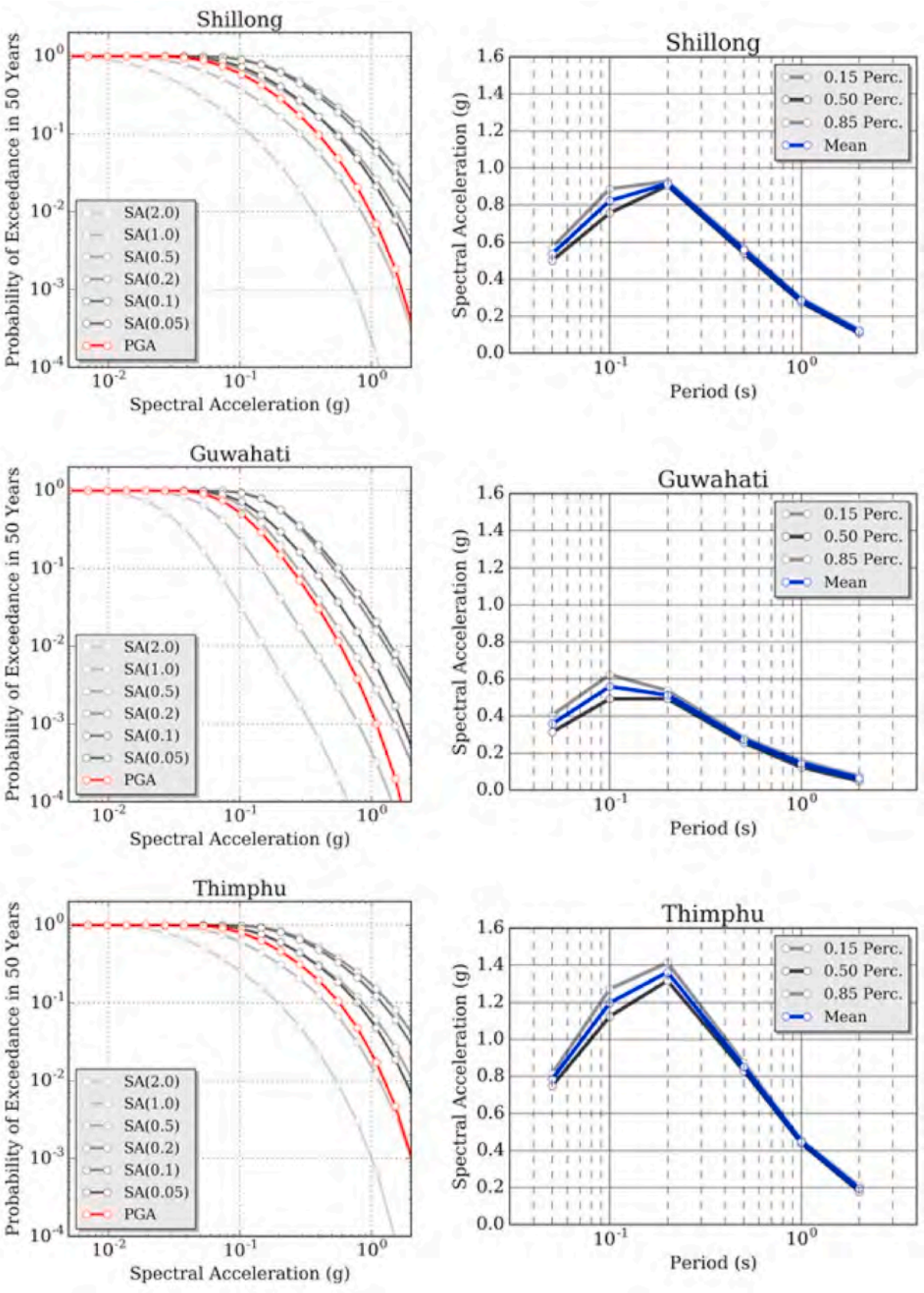

Fig. 16. Calculation with the area sources and the faults (hybrid model): on the left, the mean hazard curves computed for a range of spectral periods, including PGA; on the right, the mean and quantile UHS for different cities for 10% POE in 50 years.

hazard with the maximum PGA of 0.77 g in the northeastern part. Looking at these results, it is very clear why is so important to compute a model considering both types of sources. Like in the previous cases, Fig. 16 shows the hazard curves and UHS for Shillong city where the PGA is 0.55 g and the maximum mean SA recorded is around 0.9 g at 0.2 s. The PGA recorded is in the middle between the results for the calculations with only the area sources (0.28 g) and only the faults (0.90 g). The answer for these observations can be find in how the hybrid model is developed using different thresholds of magnitudes between the two sources.

In addition, in Fig. 16 the hazard curves, for different spectral accelerations, and the UHS for other two cities are shown. For Guwahati, the PGA is 0.35 g and the maximum mean SA is 0.55 g at 0.1 s; for Thimphu the PGA is 0.78 g and the maximum mean SA is 1.35 g at 0.2 s.

7. Discussion and conclusions

The main issue in assessing the seismic hazard in Northeast India and Bhutan is the lack of base information necessary to calibrate seismicity parameters. In particular, the availability of a sufficiently complete earthquake catalogue covering an appropriate magnitude range and time span is critical. This is however conditional to the presence of a proper local network, operational over many decades and sufficiently dense to detect down to very low-magnitude seismicity. A complete catalogue is fundamental to determine the earthquake occurrence rates, which is one of the most important parameters controlling the seismic hazard of a region. In this work we mostly relied on the information from the *Mw* homogenized ISC-GEM Extended catalogue, which is nonetheless to be considered complete only for magnitudes of 5 and above. Therefore, a possible future upgrade could be the integration of data from local seismological networks, whenever available, to supplement the available catalogue, in order to increase the total number of recorded events and consequentially perform a better statistical analysis.

Moreover, the effect of declustering is to be considered. A major assumption for the calculation of the occurrence parameters is that the earthquake generation follows a Poissonian process. For this reason, a declustering procedure based on the Gardner and Knopoff (1974) method was tested, by varying distance, magnitude and time windows. However, the classical Gardner and Knopoff (1974) method removed more than 40% of the total events, which leads to a drastic reduction of the activity rates of the source zones. A possible explanation is due to the fact that the method has been originally calibrated on data from Southern California, which is expectedly different from present study area from a geological and seismotectonics perspective. To overcome this problem, a manual procedure was performed, based on the visual selection of the cluster events, in order to have a good balance between the number of aftershocks removed and the number of the events used for the statistical analysis. The procedure has removed about 25% of the initial registered events. The choice of an optimal declustering approach is nonetheless still open issue and must be better investigated in future analysis.

Another important aspect related to the catalogue is the proper definition of the completeness periods for the different magnitudes. Several tests have been performed assuming different magnitude of completeness, both for the total study area and for each single source zone. From these tests, it was evident a strong sensitivity of this component on the final hazard results, particularly about the variability of the occurrence rates, probably due to the spatially irregular distribution of events. In this study, we assumed the earthquake occurrence process to be fully represented by a double truncated Gutenberg-Richter law. Due to the lack of local events, to obtain a more robust estimate of the activity rates, a unique *b*-value was first derived using all available events for the whole investigated area. Such value (1.05) was then imposed to the different sources, allowing only the rates (then the *a*-value) to vary. For future development, however, different *b*-values should be tested, in order to better understand the sensitivity and the influence of such parameter on the computed hazard. The *a*-value was derived differently for the two sources: for what concerns the area sources, the *a*-value was obtained from the analysis of past seismicity. Conversely, the *a*-value for the faults was calculated by means of the slip rates. The uncertainties on the *a*-value for the faults are related to many factors, in particular to GPS measurements errors. Moreover, it is important to consider that part of this slip could be accommodated and converted in plastic deformation; different values of the seismic coupling coefficient have been tested, ranging between about 10% and 80% of the total slip. A coefficient of 40% has finally been selected as optimal value for the region, providing the most realistic hazard scenarios. However, future tests should better consider the influence of lower slip rates values on the results. Several other aspects related to the faults, such as geometry, focal mechanisms and Mmax, have been analyzed, but their influence on the hazard results was found to be minor. This is particularly true and was actually expected for 475 years return period, but such consideration might not be applicable to longer return periods (e.g. 2% POE in 50 years). Regarding the area sources, the Mmax for each zone has been taken from the maximum recorded value adding 0.5 unit; for the faults, the procedure adopted is more complex and involves the use of specific conversion relations between fault length and magnitude. The first tests were made by using the entire fault trace, but this has led to a very high Mmax values and unrealistic seismic potential. For this reason, different alternative faults segmentation geometries have been developed, trying to limit the ruptures length and consequentially the expected Mmax for each fault based on geological field evidence from satellite images and seismicity distribution of past events. The segmentation model is unfortunately very subjective in most cases, but it has also a relevant impact on the hazard. A possible follow-up of this study could be the analysis of different traces segmentation to compare how this aspect influence the hazard, which has been investigated only marginally in this study due to time constraints.

A final critical element is represented by the selection of the Ground Motion Prediction Equations. Since all the area sources and the faults have been modelled like active shallow crust (except for the Burmese Arc zone that has been modelled like subduction zone), a preliminary selection of the GMPEs has verted to the equations calibrated and suitable for these tectonic frameworks. Then eleven GMPEs have been selected and tested basing on the magnitude range of operation. A logic-tree scheme was implemented in *OpenQuake* in order to account for epistemic uncertainty, using the three relations that have been considered suitable for the study area. We found that the choice of the GMPEs heavily affect the hazard results: for these reasons could be useful a future investigation where different equations and branching levels were adopted. It must be noted that the need of a logic-tree scheme is also due to the fact that there are no GMPEs calibrated on local settings, since few data of the study region are available. An important future development could therefore consist in creating a GMPE specific the Himalayan region, perhaps compensating the lack of earthquake observations with the results from numerical modelling.

Another aspect that we notice looking at Fig. 12 is the fact that the ground motion calculated doesn't change along the thrust dip direction. This problem could find an explanation in what type of distance metric is used in the GMPEs selected. For the faults, Boore et al. (2014) and Boore and Atkinson (2008) have been used and these relations are based on the Joyner-Boore distance metric (Rjb). The Rjb is defined as the shortest distance from a site to the surface projection of the rupture surface, and in practice the faults dip values have not very great effects on the ground motion results. As in the area source model, the recurrence values are the parameters that mostly drive the hazard results; however, in the faults source model, also the dip and the geometry of fault are very important for the hazard calculation.

After all the previous considerations, the overall hazard distribution in the study area reflects the seismic zonation of the Indian building code. The Bureau of Indian Standards (BIS, 2002) classifies the entire N-E India region into Zone V, that represents the highest hazard in India.

Table 4
Comparison of computed PGA (in g) with other studies for 10% probability of exceedance in 50 years (475 years return period) at selected cities.

	Shillong	Guwahati	Thimphu
Bhatia et al. (1999)	0.30	0.30	/
BIS (2002)	0.18	0.18	/
Sharma and Malik (2006)	0.45	0.50	/
NDMA (2011)	0.25	0.23	/
Nath and Thingbaija (2012)	0.72	0.66	/
Das et al. (2016)	0.32	0.24	/
Baro et al. (2018) DSHA	0.36	/	/
Baro et al. (2020)	0.19	/	/
Stevens et al. (2020)	/	/	0.77
Present study (hybrid model)	0.55	0.35	0.78

The analysis performed in this work allows obtaining a more accurate representation of the hazard level in this region. As it can be seen in Fig. 15, the state of Arunachal Pradesh has seismically higher hazard than in the Assam and Meghalaya states. The higher values in the north part of the study area are due to the presence of the Himalayan décollement (and consequently to the high values of slip in this area). In the Assam and Meghalaya states the seismic hazard increases significantly when active faults are considered.

Different studies have been carried out at regional scale and a comparison of the PGA results for Shillong, Guwahati and Thimphu between previous studies and the present investigation is shown in Table 4.

1. Khattri et al. (1984) compute a maximum PGA of 0.8 g along the Brahmaputra valley and 0.4 g–0.6 g along the Himalayan mountain belt, for the calculation at 10% probability of exceedance in 50 years, using 24 seismogenic sources for the entire India.
2. Bhatia et al. (1999) and Giardini et al. (1999), under the Global Seismic Hazard Assessment Program (GSHAP), develop a seismic hazard map for the whole India, using 86 seismic source zones. The highest values of PGA (0.35 g–0.4 g for 10% probability of exceedance in 50 years) are shown in the seismically active regions as the Burmese arc, Northeastern India and North-West Himalaya (Hindukush).
3. Walling and Mohanty (2009) give an overview on the development of the seismic zonation map of India through time as well as a review of seismic hazard and zoning studies; they point out that the seismic zonation at a national level is not sufficient for a detailed seismic hazard assessment at the local level.
4. NDMA (2011) report describes PGA values up to 0.35 g with 10% probability for exceedance in 50 years for the eastern Himalaya syntaxis and the Indo-Burmese arc. In the model, 32 source zones are modelled.
5. Nath and Thingbaijam (2012) show hazard distribution in the country significantly higher than GSHAP, and BIS (2002) studies. The highest values are shown in northeastern India.

All these previous studies are performed for the whole India, using only the area source model approach and often applying only a single attenuation relationship, disregarding the different geological provinces. For these reasons, the detailed level of the hazard results is lower with respect to the one analyzed in this study. In addition, it is important to mention some seismic hazard studies that they focus on the same study area at local scale:

1. Sharma and Malik (2006) study applies an area source model approach, and it shows PGA values between 0.05 g and 0.6 g for 475 years return period, with the maximum values occurring around the Dauki fault in the Shillong massif.
2. Das et al. (2016) perform a PSHA for Northeast India region using the area sources model approach.
3. Baro et al. (2018) carry out a Deterministic Seismic Hazard Assessment (DSHA) of the Shillong Plateau; the hazard map underlines a strong influence of the Oldham and Dauki faults on the results,
4. Baro et al. (2020) present a PSHA of Shillong Plateau, using historical and instrumentally recorded regional earthquakes since 1411.
5. Stevens et al. (2020) is the first PSHA focusing on Bhutan and it is based on faults locations, slip-rates and paleoseismic earthquake data. The results show a non-uniform hazard level across the country; this outcome goes against the existing building code of Bhutan, adopted from the Indian Seismic Zonation of 2002 (BIS- 2002), that uses a PGA of 0.36 g uniformly applied across the entire country. The PGA for Thimphu, computed for 475 years return period, is in accordance with the value calculated in the present study.

It is important to underline some aspects: the seismic hazard gap of Bhutan and the lower values obtained, compared to the ones calculated in this work. Both these facts can be attributed to the lack of faults modelling, that leads to lower and maybe not realistic PGA values. In particular, in this study, for Bhutan the hazard is driven by the Himalayan thrust. In the calculation, however, the ground motion doesn't actually change along the thrust dip direction, as it would intuitively be. As already explain, the faults dip values have not very great effects on the ground motion results due to how the considered GMPEs were built. If a specific GMPE calibrated for this zone should be consider, probably a hypocentral distance metric could lead to better results with respect to the classical Rjb used in Boore et al. (2014) and Boore and Atkinson (2008) equations.

Furthermore, there is still a long way to go with respect to understanding (and thereby predicting in more detail) the tectonic processes in this region, which is more complicated than in most other regions of the world. The conducted study represents a first step towards estimating seismic hazard for North-East India and Bhutan. However, the doubt that all the seismogenic faults have not been analyzed and taken into consideration remains; in this area, which is very complex from the geological point of view, there are most certainly many hidden seismogenic faults.

Finally, it is here important to note how the hybrid model is built. Since there are two different type of sources, the areas and the faults, it was decided to assign the basic seismicity to the area sources, with an equal distribution of the seismic potential determined through the occurrence parameters calculated for each zone. The most relevant events are instead addressed to the faults. In order to consider only once the effects of each source, the influence of the areas is limited to a magnitude of 6.5, while the potential related to the faults is set from this magnitude to the maximum magnitude calculated specifically for each fault. The seismic hazard values calculated (maximum PGA equal to 0.77 g in the hybrid model) can be used like a basis for future applications, like input data for a probabilistic risk computation and for a better definition of scenario earthquakes for deterministic risk assessment.

Data Availability

The moment tensor from the Global Centroid Moment Tensor catalogue (Ekström et al., 2012) was obtained from https://www.globalcmt.org/CMTsearch.html (last access January 2019).

The USGS earthquake catalogue was obtained from https://earthquake.usgs.gov/earthquakes/search/(last access January 2019).

The faults information was taken from the Geological Survey of India https://www.gsi.gov.in/(last access January 2019).

The Ground Motion Prediction Equations (GMPEs) (Douglas, 2019) were extracted from http://www.gmpe.org.uk (last update December 19, 2019).

OpenQuake (OQ) software (Version 2.7) was used for the computation (GEM, 2017).

Funding

This work has been performed during an Erasmus Traneeship Program and the work has been partially funded by the University of Pavia and NORSAR to cover mainly personal costs (place to stay, food and transportation) during that period.

CRediT authorship contribution statement

Federica Ghione: Conceptualization, Methodology, Software, Formal analysis, Investigation, Writing – original draft, Writing – review & editing. **Valerio Poggi:** Validation, Resources, Data curation, Supervision. **Conrad Lindholm:** Resources, Supervision.

Declaration of competing interest

The authors declare that they have no known competing financial interests or personal relationships that could have appeared to influence the work reported in this paper.

Acknowledgments

This study is made possible by the generous support of NORSAR, that provided technical assistant and scientific discussions.

References

Akinci, A., Galadini, F., Pantosti, D., Petersen, M., Malagnini, L., Perkins, D., 2009. Effect of time dependence on probabilistic seismic-hazard maps and deaggregation for the central Apennines, Italy. Bull. Seismol. Soc. Am. https://doi.org/10.1785/0120080053.

Anderson, J.G., Luco, J.E., 1983. Consequences of slip rate constants on earthquake occurrence relations. Bull. Seismol. Soc. Am. 73, 471–496.

Armijo, R., Tapponnier, P., Han, T., 1989. Late Cenozoic right-lateral strike-slip faulting in southern Tibet. J. Geophys. Res. Solid Earth 94, 2787–2838. https://doi.org/10.1029/JB094iB03p02787.

Atkinson, G.M., Boore, D.M., 2003. Empirical ground-motion relations for subduction-zone earthquakes and their application to cascadia and other regions. Bull. Seismol. Soc. Am. 93, 1703–1729. https://doi.org/10.1785/0120020156.

Barman, P., Jade, S., Shrungeshwara, T.S., Kumar, A., Bhattacharyya, S., Ray, J.D., Jagannathan, S., Jamir, W.M., 2017. Crustal deformation rates in Assam valley, Shillong Plateau, eastern Himalaya, and Indo-Burmese region from 11 years (2002–2013) of GPS measurements. Int. J. Earth Sci. 106, 2025–2038. https://doi.org/10.1007/s00531-016-1407-z.

Baro, O., Kumar, A., 2017. Seismic source characterization for the Shillong Plateau in northeast India. J. Seismol. 21, 1229–1249. https://doi.org/10.1007/s10950-017-9664-2.

Baro, O., Kumar, A., Ismail-Zadeh, A., 2020. Seismic hazard assessment of the Shillong Plateau using a probabilistic approach. Geomatics, Nat. Hazards Risk 11, 2210–2238. https://doi.org/10.1080/19475705.2020.1833989.

Baro, O., Kumar, A., Ismail-Zadeh, A., 2018. Seismic hazard assessment of the Shillong plateau, India. Geomatics. Nat. Hazards Risk. https://doi.org/10.1080/19475705.2018.1494043.

Baruah, Santanu, Baruah, Saurabh, Saikia, S., Shrivastava, M.N., Sharma, A., Reddy, C. D., Kayal, J.R., 2016. State of tectonic stress in Shillong Plateau of northeast India. Phys. Chem. Earth, Parts A/B/C 95, 36–49. https://doi.org/10.1016/j.pce.2015.11.009.

Berthet, T., Ritz, J.-F., Ferry, M., Pelgay, P., Cattin, R., Drukpa, D., Braucher, R., Hetenyi, G., 2014. Active tectonics of the eastern Himalaya: new constraints from the first tectonic geomorphology study in southern Bhutan. Geology 42, 427–430. https://doi.org/10.1130/G35162.1.

Bhatia, S.C., Kumar, M.R., Gupta, H.K., 1999. A probabilistic seismic hazard map of India and adjoining regions. Ann. Geofisc. 42, 1153–1166.

Bilham, R., England, P., 2001. Plateau 'pop-up' in the great 1897 Assam earthquake. Nature 410, 806–809. https://doi.org/10.1038/35071057.

BIS, 2002. IS 1893–2002 (Part 1): Indian Standard Criteria for earthquake resistant design of structures, Part 1—General Provisions and Buildings. Bureau of Indian Standards, New Delhi.

Boore, D.M., Atkinson, G.M., 2008. Ground-motion prediction equations for the average horizontal component of PGA, PGV, and 5%-damped PSA at spectral periods between 0.01 s and 10.0 s. Earthq. Spectra 24, 99–138. https://doi.org/10.1193/1.2830434.

Boore, D.M., Stewart, J.P., Seyhan, E., Atkinson, G.M., 2014. NGA-West2 equations for predicting PGA, PGV, and 5% damped PSA for shallow crustal earthquakes. Earthq. Spectra 30, 1057–1085. https://doi.org/10.1193/070113EQS184M.

Bungum, H., 2007. Numerical modelling of fault activities. Comput. Geosci. 33, 808–820. https://doi.org/10.1016/j.cageo.2006.10.011.

Bungum, H., Lindholm, C.D., Mahajan, A.K., 2017. Earthquake recurrence in NW and central Himalaya. J. Asian Earth Sci. https://doi.org/10.1016/j.jseaes.2017.01.034.

Carlton, B.D., Skurtveit, E., Bohloli, B., Atakan, K., Dondzila, E., Kaynia, A.M., 2018. Probabilistic seismic hazard analysis for offshore bangladesh including fault sources. https://doi.org/10.1061/9780784481462.015.

Cornell, C.A., 1968. Engineering seismic risk analysis. Bull. Seismol. Soc. Am. 58, 1583–1606.

Curray, J.R., Emmel, F.J., Moore, D.G., Raitt, R.W., 1982. Structure, tectonics, and geological history of the northeastern Indian ocean. In: The Ocean Basins and Margins. Springer US, Boston, MA, pp. 399–450. https://doi.org/10.1007/978-1-4615-8038-6_9.

Curray, J.R., Moore, D.G., Lawver, L.A., Emmel, F.J., Raitt, R.W., Henry, M., Kieckhefer, R., 1979. Tectonics of the andaman sea and Burma. In: Geological and Geophysical Investigations of Continental Margins. American Association of Petroleum Geologists, pp. 189–198.

Das, R., Sharma, M.L., Wason, H.R., 2016. Probabilistic seismic hazard assessment for Northeast India region. Pure Appl. Geophys. 173, 2653–2670. https://doi.org/10.1007/s00024-016-1333-9.

De, R., Kayal, J.R., 2003. Seismotectonic model of the Sikkim Himalaya: constraint from microearthquake surveys. Bull. Seismol. Soc. Am. 93, 1395–1400. https://doi.org/10.1785/0120020211.

Diehl, T., Singer, J., Hetényi, G., Grujic, D., Clinton, J., Giardini, D., Kissling, E., 2017. Seismotectonics of Bhutan: evidence for segmentation of the Eastern Himalayas and link to foreland deformation. Earth Planet Sci. Lett. 471, 54–64. https://doi.org/10.1016/j.epsl.2017.04.038.

Douglas, J., 2019. Ground motion prediction equations 1964-2019 [WWW Document]. URL. http://www.gmpe.org.uk/gmpereport2014.pdf.

Ekström, G., Nettles, M., Dziewoński, A.M., 2012. The global CMT project 2004–2010: Centroid-moment tensors for 13,017 earthquakes. Phys. Earth Planet. Inter. 200–201, 1–9. https://doi.org/10.1016/j.pepi.2012.04.002.

England, P., Bilham, R., 2015. The Shillong Plateau and the great 1897 Assam earthquake. Tectonics 34, 1792–1812. https://doi.org/10.1002/2015TC003902.

Esteva, L., 1968. Bases para la formulacion de decisiones de diseño sísmico. Universidad Autonoma Nacional de México.

Esteva, L., 1967. Criterios para la construcción de espectros para diseño sísmico, Proceedings of the XII Jornadas Sudamericanas de Ingeniería Estructural y III Simposio Panamericano de Estructuras. Published later in Boletín del Instituto de Materiales y Modelos Estructurales, 19. Universidad Central de Venezuela, 1967., Caracas.

Gahalaut, V.K., Rajput, S., Kundu, B., 2011. Low seismicity in the Bhutan Himalaya and the stress shadow of the 1897 Shillong Plateau earthquake. Phys. Earth Planet. In. 186, 97–102. https://doi.org/10.1016/j.pepi.2011.04.009.

Gardner, J.K., Knopoff, L., 1974. Is the sequence of earthquakes in southern California, with aftershock removed, Poissonian? Bull. Seismol. Soc. Am. 64, 1363–1367.

GEM, 2017. The OpenQuake-engine user manual. Global Earthquake Model (GEM) Technical Report 2017-11. https://doi.org/10.13117/GEM.OPENQUAKE.MAN.ENGINE.2.8/01.

Giardini, D., Grünthal, G., Shedlock, K.M., Zhang, P., 1999. The GSHAP global seismic hazard map. Ann. Geofisc. 42, 1225–1228.

Goswami, S., 2005. Inverted metamorphism in the Sikkim-Darjeeling Himalaya: structural, metamorphic and numerical studies. University of Cambridge.

Greenwood, L.V., Argles, T.W., Parrish, R.R., Harris, N.B.W., Warren, C., 2016. The geology and tectonics of central Bhutan. J. Geol. Soc. London. 173, 352–369. https://doi.org/10.1144/jgs2015-031.

Gulia, L., Wiemer, S., Wyss, M., 2012. Theme IV–understanding seismicity catalog artifacts and quality control. Community Online Resour. Stat. Seism. Anal. 1–26 https://doi.org/10.5078/corssa-93722864.

Gutenberg, B., Richter, C.F., 1956. Magnitude and energy of earthquakes. Ann. Geofisc. 9, 1–15.

Hainzl, S., Scherbaum, F., Beauval, C., 2006. Estimating background activity based on interevent-time distribution. Bull. Seismol. Soc. Am. https://doi.org/10.1785/0120050053.

Hauck, M.L., Nelson, K.D., Brown, L.D., Zhao, W., Ross, A.R., 1998. Crustal structure of the Himalayan orogen at ~90° east longitude from Project INDEPTH deep reflection profiles. Tectonics 17, 481–500. https://doi.org/10.1029/98TC01314.

Hetényi, G., Le Roux-Mallouf, R., Berthet, T., Cattin, R., Cauzzi, C., Phuntsho, K., Grolimund, R., 2016. Joint approach combining damage and paleoseismology observations constrains the 1714 A.D. Bhutan earthquake at magnitude 8 ± 0.5. Geophys. Res. Lett. 43 https://doi.org/10.1002/2016GL071033, 10,695-10,702.

Imsong, W., Choudhury, S., Phukan, S., 2016. Ascertaining the neotectonic activities in the southern part of Shillong Plateau through geomorphic parameters and remote sensing data. Curr. Sci. 110, 91. https://doi.org/10.18520/cs/v110/i1/91-98.

Islam, M.S., Shinjo, R., Kayal, J.R., 2011. Pop-up tectonics of the Shillong Plateau in northeastern India: insight from numerical simulations. Gondwana Res. 20, 395–404. https://doi.org/10.1016/j.gr.2010.11.007.

Kanamori, H., Anderson, D.L., 1975. Theoretical basis of some empirical relations in seismology. Bull. Seismol. Soc. Am. 65, 1073–1095.

Kaverina, A.N., Lander, A.V., Prozorov, A.G., 1996. Global creepex distribution and its relation to earthquake-source geometry and tectonic origin. Geophys. J. Int. 125, 249–265. https://doi.org/10.1111/j.1365-246X.1996.tb06549.x.

Kayal, J.R., 2010. Himalayan tectonic model and the great earthquakes: an appraisal. Geomatics, Nat. Hazards Risk 1, 51–67. https://doi.org/10.1080/19475701003625752.

Kayal, J.R., 2008. Microearthquake Seismology and Seismotectonics of South Asia. Springer.

Kayal, J.R., Arefiev, S.S., Barua, S., Hazarika, D., Gogoi, N., Kumar, A., Chowdhury, S.N., Kalita, S., 2006. Shillong plateau earthquakes in northeast India region: complex tectonic model. Curr. Sci. 91, 109–114.
Khattri, K.N., Rogers, A.M., Perkins, D.M., Algermissen, S.T., 1984. A seismic hazard map of India and adjacent areas. Tectonophysics. https://doi.org/10.1016/0040-1951(84)90156-2.
Lavé, J., Avouac, J.P., 2000. Active folding of fluvial terraces across the siwaliks hills, Himalayas of central Nepal. J. Geophys. Res. Solid Earth 105, 5735–5770. https://doi.org/10.1029/1999JB900292.
Le Dain, A.Y., Tapponnier, P., Molnar, P., 1984. Active faulting and tectonics of Burma and surrounding regions. J. Geophys. Res. 89, 453. https://doi.org/10.1029/JB089iB01p00453.
Le Roux-Mallouf, R., Godard, V., Cattin, R., Ferry, M., Gyeltshen, J., Ritz, J.F., Drupka, D., Guillou, V., Arnold, M., Aumaître, G., Bourlès, D.L., Keddadouche, K., 2015. Evidence for a wide and gently dipping Main Himalayan Thrust in western Bhutan. Geophys. Res. Lett. 42, 3257–3265. https://doi.org/10.1002/2015GL063767.
Marechal, A., Mazzotti, S., Cattin, R., Cazes, G., Vernant, P., Drukpa, D., Thinley, K., Tarayoun, A., Le Roux-Mallouf, R., Thapa, B.B., Pelgay, P., Gyeltshen, J., Doerflinger, E., Gautier, S., 2016. Evidence of interseismic coupling variations along the Bhutan Himalayan arc from new GPS data. Geophys. Res. Lett. 43 https://doi.org/10.1002/2016GL071163, 12,399-12,406.
Martin, S., Szeliga, W., 2010. A catalog of felt intensity data for 570 earthquakes in India from 1636 to 2009. Bull. Seismol. Soc. Am. 100, 562–569. https://doi.org/10.1785/0120080328.
Mitchell, A.H.G., McKerrow, W.S., 1975. Analogous evolution of the Burma orogen and the scottish caledonides. Geol. Soc. Am. Bull. 86, 305. https://doi.org/10.1130/0016-7606(1975)86<305:AEOTBO>2.0.CO;2.
Murray, J.R., Minson, S.E., Svarc, J.L., 2014. Slip rates and spatially variable creep on faults of the northern San Andreas system inferred through bayesian inversion of global positioning system data. J. Geophys. Res. Solid Earth. https://doi.org/10.1002/2014JB010966.
Nandy, D.R., 2001. Geodynamics of Northeastern India and the Adjoining Region. ACB Publication, Kolkata.
Nandy, D.R., 1983. The eastern Himalaya and the Indo-Burman Orogen in relation to the Indian plate movement. Geol. Surv. India Misc. Pub. 43, 153–159.
Nath, S.K., Thingbaijam, K.K.S., 2012. Probabilistic seismic hazard assessment of India. Seismol Res. Lett. https://doi.org/10.1785/gssrl.83.1.135.
NDMA, 2011. Development of probabilistic seismic hazard map of India technical report. Natl. Dis. Manag. Auth.
Oldham, R.D., 1899. Report on the great earthquake of the 12th June 1897, in: Geological Survey of India Mem, p. 379.
Panzera, F., Zechar, J.D., Vogfjörd, K.S., Eberhard, D.A.J., 2016. A revised earthquake catalogue for south Iceland. Pure Appl. Geophys. 173, 97–116. https://doi.org/10.1007/s00024-015-1115-9.
Paul Burgess, W., Yin, A., Dubey, C.S., Shen, Z.-K., Kelty, T.K., 2012. Holocene shortening across the main frontal thrust zone in the eastern Himalaya. Earth Planet Sci. Lett. 357–358, 152–167. https://doi.org/10.1016/j.epsl.2012.09.040.
Poggi, V., Garcia-Peláez, J., Styron, R., Pagani, M., Gee, R., 2020. A probabilistic seismic hazard model for North Africa, Bulletin of Earthquake Engineering. Springer Netherlands. https://doi.org/10.1007/s10518-020-00820-4.
Rajendran, C.P., Rajendran, K., Duarah, B.P., Baruah, S., Earnest, A., 2004. Interpreting the style of faulting and paleoseismicity associated with the 1897 Shillong, northeast India, earthquake: implications for regional tectonism. Tectonics 23. https://doi.org/10.1029/2003TC001605.
Rivas-Medina, A., Benito, B., Gaspar-Escribano, J.M., 2018. Approach for combining fault and area sources in seismic hazard assessment: application in south-eastern Spain. Nat. Hazards Earth Syst. Sci. 18, 2809–2823. https://doi.org/10.5194/nhess-18-2809-2018.
Saikia, S., Chopra, S., Baruah, S., Singh, U.K., 2017. Shallow sedimentary structure of the Brahmaputra valley constraint from receiver functions analysis. Pure Appl. Geophys. 174, 229–247. https://doi.org/10.1007/s00024-016-1371-3.
Seeber, L., Armbruster, J.G., Quittmeyer, R., 1981. Seismicity and continental subduction in the Himalayan arc. Himalaya Geodyn. Evol. 4, 215–242.
Sharma, A., Baruah, S., Piccinini, D., Saikia, S., Phukan, M.K., Chetia, M., Kayal, J.R., 2017. Crustal seismic anisotropy beneath Shillong plateau - Assam valley in North East India: shear-wave splitting analysis using local earthquakes. Tectonophysics 717, 425–432. https://doi.org/10.1016/j.tecto.2017.08.027.
Sharma, M.L., Malik, S., 2006. Probabilistic seismic hazard analysis and estimation of spectral strong ground motion on bed rock in North East India. 4th Int. Conf. Earthq. Eng. Taipei, Taiwan.
Shivamanth, A., Shama, P.S., K, D., M, S., C, H., 2016. A review on development of seismic hazard analysis of India. Int. J. Mod. Trends Eng. Res. 3.
Stepp, J.C., 1971. An investigation of earthquake risk in the Puget Sound area by use of the type I distribution of largest extremes. Pennsylvania State University.
Stevens, V.L., Avouac, J.P., 2015. Interseismic coupling on the main Himalayan thrust. Geophys. Res. Lett. 42, 5828–5837. https://doi.org/10.1002/2015GL064845.
Stevens, V.L., De Risi, R., Le Roux-Mallouf, R., Drukpa, D., Hetényi, G., 2020. Seismic hazard and risk in Bhutan. Nat. Hazards. https://doi.org/10.1007/s11069-020-04275-3.
Tapponnier, P., Peltzer, G., Le Dain, A.Y., Armijo, R., Cobbold, P., 1982. Propagating extrusion tectonics in Asia: new insights from simple experiments with plasticine. Geology 10, 611. https://doi.org/10.1130/0091-7613(1982)10<611:PETIAN>2.0.CO;2.
Taroni, M., Akinci, A., 2021. Good practices in PSHA: declustering, b-value estimation, foreshocks and aftershocks inclusion; A case study in Italy. Geophys. J. Int. https://doi.org/10.1093/gji/ggaa462.
Thatcher, W., Pollitz, F.F., 2008. Temporal evolution of continental lithospheric strength in actively deforming regions. GSA Today (Geol. Soc. Am.). https://doi.org/10.1130/GSAT01804-5A.1.
Uyeda, S., Kanamori, H., 1979. Back-arc opening and mode of subduction. J. Geophys. Res. 84, 1049–1061.
Valentini, A., Pace, B., Boncio, P., Visini, F., Pagliaroli, A., Pergalani, F., 2019. Definition of seismic input from fault-based PSHA: remarks after the 2016 Central Italy earthquake sequence. Tectonics. https://doi.org/10.1029/2018TC005086.
Valentini, A., Visini, F., Pace, B., 2017. Integrating faults and past earthquakes into a probabilistic seismic hazard model for peninsular Italy. Nat. Hazards Earth Syst. Sci. https://doi.org/10.5194/nhess-17-2017-2017.
Velasco, A.A., Gee, V.L., Rowe, C., Grujic, D., Hollister, L.S., Hernandez, D., Miller, K.C., Tobgay, T., Fort, M., Harder, S., 2007. Using small, temporary seismic networks for investigating tectonic deformation: brittle deformation and evidence for strike-slip faulting in Bhutan. Seismol Res. Lett. 78, 446–453. https://doi.org/10.1785/gssrl.78.4.446.
Vernant, P., Bilham, R., Szeliga, W., Drupka, D., Kalita, S., Bhattacharyya, A.K., Gaur, V. K., Pelgay, P., Cattin, R., Berthet, T., 2014. Clockwise rotation of the Brahmaputra valley relative to India: tectonic convergence in the eastern Himalaya, naga hills, and Shillong Plateau. J. Geophys. Res. Solid Earth 119, 6558–6571. https://doi.org/10.1002/2014JB011196.
Vorobieva, I., Mandal, P., Gorshkov, A., 2017. Block-and-fault dynamics modelling of the Himalayan frontal arc: implications for seismic cycle, slip deficit, and great earthquakes. J. Asian Earth Sci. 148, 131–141. https://doi.org/10.1016/j.jseaes.2017.08.033.
Walling, M.Y., Mohanty, W.K., 2009. An overview on the seismic zonation and microzonation studies in India. Earth Sci. Rev. https://doi.org/10.1016/j.earscirev.2009.05.002.
Weatherill, G.A., Pagani, M., Garcia, J., 2016. Exploring earthquake databases for the creation of magnitude-homogeneous catalogues: tools for application on a regional and global scale. Geophys. J. Int. 206, 1652–1676. https://doi.org/10.1093/gji/ggw232.
Wells, D.L., Coppersmith, K.J., 1994. New empirical relationships among magnitude, rupture length, rupture width, rupture area, and surface displacement. Bull. Seismol. Soc. Am. 84, 974–1002.
Woessner, J., Laurentiu, D., Giardini, D., Crowley, H., Cotton, F., Grünthal, G., Valensise, G., Arvidsson, R., Basili, R., Demircioglu, M.B., Hiemer, S., Meletti, C., Musson, R.W., Rovida, A.N., Sesetyan, K., Stucchi, M., Anastasiadis, A., Akkar, S., Engin Bal, I., Barba, S., Bard, P.Y., Beauval, C., Bolliger, M., Bosse, C., Bonjour, C., Bungum, H., Carafa, M., Cameelbeeck, T., Carvalho, A., Campos-Costa, A., Coelho, E., Colombi, M., D'amico, V., Devoti, R., Drouet, S., Douglas, J., Edwards, B., Erdik, M., Fäh, D., Fonseca, J., Fotopoulou, S., Glavatovic, B., Gómez Capera, A.A., Hauser, J., Husson, F., Kastelic, V., Kästli, P., Karatzetzou, A., Kaviris, G., Keller, N., Kierulf, H.P., Kouskouna, V., Krishnamurty, R., Lang, D., Lemoine, A., Lindholm, C., Makropoulos, K., Manakou, M., Marmureanu, G., Martinelli, F., Garcia Mayordomo, J., Mihaljevic, J., Monelli, D., Garcia-Moreno, D., Nemser, E., Pagani, M., Pinho, R., Pisani, A.R., Pitilakis, D., Pitilakis, K., Poggi, V., Radulian, M., Riga, E., Sandikkaya, M.A., Segou, M., Siegert, R., Silva, V., Stromeyer, D., Sousa, L., Sørensen, M.B., Tellez-Arenas, A., Vanneste, K., Wahlström, R., Weatherill, G., Viganò, D., Vilanova, S., Yenier, E., Zulfikar, C., Adams, J., Bommer, J.J., Bonilla, F., Faccioli, E., Gülen, L., Koller, M., Pinto, A., Pinto, P., Papaioannou, C., Peruzza, L., Scherbaum, F., Scotti, O., Stirling, M., Theodoulidis, N., Wenk, T., Zschau, J., 2015. The 2013 European Seismic Hazard Model: key components and results. Bull. Earthq. Eng. https://doi.org/10.1007/s10518-015-9795-1.
Yadav, R.B.S., Tripathi, J.N., Rastogi, B.K., Das, M.C., Chopra, S., 2010. Probabilistic assessment of earthquake recurrence in northeast India and adjoining regions. Pure Appl. Geophys. 167, 1331–1342. https://doi.org/10.1007/s00024-010-0105-1.
Yaghmaei-Sabegh, S., Shoaeifar, N., Shoaeifar, P., 2018. A bimodal hybrid model for time-dependent probabilistic seismic hazard analysis. Pure Appl. https://doi.org/10.1007/s00024-018-1839-4. Geophys.
Yin, A., 2006. Cenozoic tectonic evolution of the Himalayan orogen as constrained by along-strike variation of structural geometry, exhumation history, and foreland sedimentation. Earth Sci. Rev. 76, 1–131. https://doi.org/10.1016/j.earscirev.2005.05.004.
Youngs, R.R., Coppersmith, K.J., 1985. Implications of fault slip rates and earthquake recurrence models to probabilistic seismic hazard estimates. Bull. Seismol. Soc. Am. 75, 939–964.
Zhang, L., Li, J., Liao, W., Wang, Q., 2016. Source rupture process of the 2015 Gorkha, Nepal Mw7.9 earthquake and its tectonic implications. Geod. Geodyn. 7, 124–131. https://doi.org/10.1016/j.geog.2016.03.001.
Zhuang, J., Ogata, Y., Vere-Jones, D., 2002. Stochastic declustering of space-time earthquake occurrences. J. Am. Stat. Assoc. https://doi.org/10.1198/016214502760046925.